2008

High throughput fermentation monitoring via bubble detection

Jasjeet Kaur
Iowa State University

High throughput fermentation monitoring via bubble detection

by

Jasjeet Kaur

A thesis submitted to the graduate faculty

in partial fulfillment of the requirements for the degree of

MASTER OF SCIENCE

Major: Agricultural Engineering

Program of Study Committee:

D. Raj Raman, Major Professor

Robert P. Anex

Steven J. Hoff

Iowa State University

Ames, Iowa

2008

DEDICATIONS

I would like to dedicate this work as a thanksgiving to the Lord for all his blessings that he has showered upon me, without which this work would not have been possible. I would also like to dedicate this work to my mother, Ranjeet Kaur; my father, Charanjeet Singh; my brother, Harsimran Singh; my Grandmother; my late Grandfather and a very special person, Sukhdeep Singh for all of their support and prayers.

TABLE OF CONTENTS

LIST OF FIGURES

LIST OF TABLES

ACKNOWLEDGEMENTS

I would like to express my sincere appreciation and thanks to my major professor, Dr. Raj Raman, for his support and guidance throughout my studies at Iowa State University. His efforts and guidance helped me in the completion of my thesis and provided me an opportunity to have an experience in the research field.

I would also like to thank my committee members, Drs. Robert. P. Anex and Steven. J. Hoff, for their support and guidance through my academic and research work. I appreciate their role of being my committee members throughout my Masters program.

Also, I am very thankful to all of the people especially, Alex Duetmeyer, Siva Sudani, Vineeth Kisara, and Raj Raman who provided programming support for my research work. In addition, I would like to thank Raman/Anex lab group members for providing help in my research project.

Last but not the least, I would take an opportunity to thank my parents and friends for their support and encouragement which have helped me overcome many obstacles during my academic career, and above all I am very grateful to God for providing me strength throughout my life.

CHAPTER 1
INTRODUCTION

Modernization and rapid growth of the world population in recent years have increased the energy demand for every day purposes. Dwindling supplies of fossil fuel resources like petroleum, coal and natural gas, have increased prices and thereby affected the U.S. economy. ‘’The U.S. consumes 25% of the world’s oil resources, and imports nearly 60%’’ of this (Chen *et al*., 2007). Moreover, use of petroleum based fuels lead to greenhouse gas emissions, thus, imposing a greater risk of global warming. The transportation sector is a major energy consumer, and with the increase in the demand for transportation fuel, gasoline prices are rising due to the limited fossil fuel resources, thereby encouraging the use and production of biofuels from renewable resources like biomass (Demirbas, 2008).

Biofuels are obtained from biomass, which is a renewable energy resource. One of the biofuels currently in use is ethanol, which is a renewable fuel that can be blended with gasoline. Ethanol is readily obtained from fermentation of starches and/or sugars present in a wide range of crops (Demirbas, 2005).

The use of bioethanol as fuel in automobiles helps in the reduction of green house gases (Demirbas, 2008). The combustion of bioethanol leads to lower pollutant content as compared to fossil fuels. MTBE (Methyl tertiary butyl ether) which used to be added to gasoline as oxygenate, has been replaced by ethanol, as the former contaminates soil and water (Wang *et al*., 2007; McCarthy and Tiemann,

1998). One of the major reasons for increasing the use of biofuels is to reduce greenhouse gas emissions. On a life cycle basis, ethanol generally emits lower carbon dioxide in comparison to gasoline (Demirbas, 2008; Wang *et al*., 2007).

The “Billion Ton Study” conducted by the Department of Energy (D.O.E) during 2005 revealed that near 1.3 billion tons of biomass is available in the U.S. each year, which has enough potential to meet the U.S. fuel demand through conversion of biomass into liquid fuel. Out of this, 368 million dry tons of biomass come from forest resources and the rest consists of agricultural resources (Perlack *et al*., 2005).

Currently, U.S. fuel ethanol is produced primarily from corn to meet the growing biofuel mandated demand. The Renewable Fuel Standard (RFS) has set a volume for ethanol production to 9 billion gallons during the year 2008 and to 36 billion gallons by 2022 (RFS, 2007). The use of corn for meeting the mandated ethanol production would significantly impact food prices as it is one of the most important feed sources in U.S animal production system. Also, to meet the ethanol production target set by the RFS, more land would be needed if ethanol has to be produced from corn. Agricultural residues and other lignocellulosic feedstocks could be harnessed for the ethanol production. Most of these materials are by products from crop harvest and other forest wastes, so no additional land is required for their production (Chen *et al*., 2007). Thus, exploration of the potential feedstocks for ethanol production including lignocellulosic materials, agricultural residues, industrial wastes, etc. is ongoing. Ethanol produced from such lignocellulosic

materials is called cellulosic ethanol. Cellulose is the main structural component of plants and cannot be digested by humans, so, the utilization of these cellulosic materials for ethanol production would not directly impact the food grain demand of the U.S. Moreover, higher amounts of biomass can be produced per unit land area because the whole plant can be harvested (Brown, 2003).

Greenhouse gas emissions (GHG) from cellulosic ethanol are 90% less when compared with gasoline. This is significantly better than the GHG emissions from corn based ethanol, which are only 20% lower than gasoline (Wang, 2005). In addition, cellulosic ethanol has a five times better net energy balance than does corn-based ethanol. When used as a fuel, cellulosic ethanol releases less sulfur, carbon monoxide, particulates, and greenhouse gases (D.O.E. Office of Science, 2008).

The U.S. has a lot of potential lignocellulosic feedstock, but the technology for its efficient use and conversion into liquid fuels is still under development. Lignocellulosic materials consist of cellulose, lignin, and hemicelluloses. Lignin binds cellulose and hemicellulose and imposes a major problem during fermentation, as it is hard to break down into simpler compounds. Prior to fermentation of lignocellulosic feedstock, pretreatment is required to get simpler compounds and many different techniques are being developed for the effective breakdown of the material (Sun and Cheng, 2002; Malherbe and Cloete, 2002). In order to meet the high demand of ethanol, different varieties of feedstocks and pretreatment methods are being studied to obtain high ethanol yields.

The uses of spectrophotometric methods, gas chromatography, and the HPLC for monitoring the fermentative capability of thousands of fermentation samples involves a huge amount of investment and time in the preparation of samples by centrifugation and filtration, and are not designed to analyze hundreds of feedstock samples rapidly. In order to save time and money, a new technique for the real time monitoring of the fermentation parameters is needed. Although, numerous fermentation monitoring systems have been developed (e.g., Eliana *et al*., 2007; Lapa *et al*., 2003; Warriner *et al*., 2002; Gemeiner *et al*., 2002; Varma *et al*., 1999; Weimer *et al*., 2004), none of these methods could handle dozens of fermentations at a time while providing real time data.

A potentially cost-effective, high-throughput fermentation screening method was proposed. The system would monitor hundreds of fermentation samples in real time using relatively low cost optical sensors. If successfully developed, such a system would be an enabling technology that would help scientists to evaluate biomass feedstocks and pretreatment methods more rapidly and inexpensively. The original goal of this study was to develop a real time fermentation monitoring method based upon carbon dioxide sensing, and to test this method using different biomass materials. Because of unforeseen technical challenges, the goal was revised. The new goal was to develop a multi channel bubble-based system using an optical sensor for fermentation monitoring, and to test the system using the fermentation of simple sugars like glucose.

CHAPTER 2
LITERATURE REVIEW

The “Billion Ton Study” conducted by the Department of Energy (DOE) revealed that over 1 billion tons of lignocellulosic biomass feedstock is available in the U.S. each year (Perlack *et al*., 2005). We do not have the required technology for the economic conversion of this huge resource into ethanol, which can be used as transportation fuel. Moreover, efforts are underway to evaluate the potential of dedicated biomass feed stocks like switchgrass, hybrid poplar, and Miscanthus. Various ethanol monitoring methods have been developed to study the effectiveness of conversion of different biomass into bioethanol (e.g., Warriner *et al*., 2002; Gemeiner *et al*., 2002; Varma *et al*., 1999; Weimer *et al*., 2004).

Several direct ethanol or sugar screening methods have been developed to monitor the ethanol production during fermentation processes. For example, ethanol and glutamate contents during the fermentation were measured after a preset decrease in glucose content, which was monitored continuously using an automated multi channel flow injection system (FIA) (Chen and Matsumoto, 1995).

A sequential injection analysis system (SIA), which was a modified flow injection system, was employed for inline detection of ethanol during fermentation (Eliana *et al*., 2007). Two microreactors packed with alcohol oxidase (AOD) and horseradish peroxidase (HRP), immobilized separately on glass beads were employed with SIA. The indicator solution consisted of 4-aminophenazone 0.359 g/l

and phenol 0.875 g/l in a 0.1 M sodium phosphate buffer solution of pH 7.0. Ethanol from the fermentation was oxidized into acetaldehyde and hydrogen peroxide. Hydrogen peroxide reacted with the 4-aminophenazone, resulting in a colored product, monoimino-p-benzoquinone-4-phenazone. This colored product was then detected using a spectrophotometer at 470 nm. Ethanol was also determined using gas chromatography and HPLC. Results from the SIA and gas chromatography correlated highly (R^2= 0.99). This system performance was also evaluated for ethanol detection of distilled and non-distilled beverages and results showed less than 3 % error when compared with the HPLC data. The results from the alcoholic fermentation parameters prediction from both HPLC and SIA showed relative error less than 4.9 %. This system used a diluted sample of 1.2 ml and indicator volume of 0.14 ml for each run, and was suitable to detect fermentation parameters for a linear range of 5 mg/l – 40 mg/l ethanol (Eliana *et al*., 2007).

An SIA system based on amperometric detection system to detect glucose and ethanol was designed (Lapa *et al*., 2003). An amperometric detection system measures the current proportional to the concentration of the species generating the current. This SIA was developed on the automatic analytical strategy and used catalytic reactors of oxidase enzymes immobilized on controlled glass pore (Lapa *et al*., 2003). These approaches, although elegant in the context of detecting glucose content and other fermentation parameters for micro-reactors /bio-reactors, could only monitor one or two reactors at a time, and must have a sample from the fermentation broth for the detection of fermentation parameters. However, the

method proposed in our study eliminates the need of taking samples from the broth, and has an edge over the existing monitoring methods by real time monitoring more than one sample.

For the accurate measurement of ethanol in the presence of glucose, a *Gluconobactor oxydens* biosensor with a cellulose acetate membrane was designed. The cellulase acetate membrane obstructed the flow of glucose through it but allowed ethanol to pass through the membrane. A coating of *Gluconobactor oxydens* was applied on the glassy carbon electrode and amperometric detection was employed for biosensors measurements. This biosensor performance was not affected by the pH in the studied range of 5.0-7.0, and it had an operational stability of 8.5 h, sensitivity of 0.076 µA mg/l^{-1} with a linear range of 0.092- 12.42 mg/l and response time of 3 sec (Gemeiner *et al*., 2002). The results showed that these micro biosensors worked better than enzyme biosensors and were in excellent agreement with the HPLC results with R^2=0.99.

Furthermore, a modified poly phenyl ether sulphone (PES) microelectrode, having higher ethanol permeability than PVC membrane, and less risk of fouling at acidic conditions, allowed monitoring of fermentation at low pH. Its linear detection range of 0 -14% (v/v) and a superior thermal tolerance as compared to platinum microelectrode arrays with PVC membranes made it work well in organic solutions for the detection of ethanol (Warriner *et al*., 2002). A focused beam reflectance measurement technique using an optical probe for real time monitoring of yeast cells flocculation parameters eliminated the need of taking samples from the

fermentation broth, which would otherwise affect the shape and size distributions of the floc chord (Ge. X. M *et al.*, 2005).

A low cost optical detection system, which consisted of semiconductor light sources and detectors, was employed in measuring pH and dissolved oxygen for a low cost micro bioreactor of 2 ml working volume. The fermentation parameters data were compared with parameters from a 1 L fermentation volume of same $K_l a$ as of the microreactors ($K_l a$ is a volumetric liquid mass transfer co-efficient for the characterization of the bioreactors capacity for aeration). The results showed that the microreactors can be combined to get high throughput fermentation (Kostov *et al*., 2001). These above direct screening methods worked fine at very low concentration of ethanol and glucose levels in the fermentation broth. Also, they were designed to monitor micro or very small bio- reactors of volume nearly 2 ml to effectively detect fermentation parameters with fair correlation around R^2=0.99 with the HPLC and other analytical methods. However, these methods require sample preparation/injection from the fermentation broth and could analyze one reactor at a time. These methods are limited by the fact that real time monitoring cannot be performed with more than one reactor at a time.

In contrast to sugar screening or direct ethanol measurement, monitoring of ethanol via monitoring of carbon dioxide produced during fermentation has been used. A soap film meter consisting of a rubber bulb and soap solution was developed (Varma *et al*., 1999). This meter was connected with the immobilized yeast cell bioreactor for the ethanol production by a side arm, and was made

airtight. Displacement of soap film by the carbon dioxide production during the steady state fermentation process was noted as a measure of the carbon dioxide production rate. Also, broth samples were taken for the estimation of ethanol by gas chromatography and results were very close, with an error of 3.3 % (Varma *et al*., 1999). In another study, ethanol produced from wet oxidized corn stover by simultaneous saccharification fermentation (SSF) showed maximum yield of 84% at 30 FPU/ g DM of enzyme loading and the ethanol rate was monitored through the weight loss of the fermentation flask, which was a measure of CO_2 loss from the flask. The results showed no significant differences from the HPLC results (Varga *et al*., 2004).

Measuring the fermentative potential of various dedicated lignocellulosic feedstocks using the current analytical methods is time consuming. Capturing the gas produced in the fermentation provides an indirect way of the estimation of the ethanol and many studies on monitoring the gas production have been done. Weimer *et al*., (2004) designed an in vitro ruminal (IVR) digestion for analyzing the cellulosic fermentation. IVR assay did not require aseptic conditions, thus, a large number of samples was monitored using this IVR assay. In this case, fermentation was carried out in sealed vials and gas pressure readings were taken using a pressure gauge. The gas production value provided an indirect measure of ethanol due to 1:1 ratio between ethanol and carbon dioxide. Three types of grasses were used for both in vitro and SSF; namely, eastern gamagrass, bluestem, and switchgrass. The IVR-CO_2 assay results for 96 hours were compared with SSF

assay results for 7 days, and it was seen that there was a good correlation (R^2=0.823 – 0.909) for eastern gamagrass and bluestem. This assay used a gas detection method, and was well correlated with the actual ethanol yield.

Gunta M. *et al*., (2004) developed an online monitoring method for fermentation using mid-infrared spectroscopy. This system employed a diamond-attenuated total reflection element (ATR) enclosed in a flow cell. The design involved a completely automated, computer controlled flow system using a 5 ml syringe and a peristaltic pump. The flow system was controlled via Visual Basic 6.0 based program Sagittarius V2, which was coded in the laboratory. This flow system acted as a connector between the fermentor and the Fourier transform infrared spectrometer (FT-IR), which was equipped with the ATR element. This method was tested on the simple sugars to ethanol conversion by yeast because this conversion has widespread applications in the industry. As a reference method, HPLC analyses were employed for the determination of glucose and ethanol concentrations. Samples from the fermentation broth were taken after 20 min. Completion of one cycle took nearly the same time, so sample throughput was 3 hr^{-1}. This system was also equipped with two degassing mechanisms to remove the carbon dioxide bubbles produced by yeast cells on the ATR flow cell: a glass element was placed in front of FT-IR spectrometer in such a manner that the solution was divided into two parts and the degassed flow was sent to the ATR element. The problem of biofilm formation over the ATR element was reduced by including a cleaning step by using 5% $NaHCO_3$ followed by distilled water circulated over the ATR element. The

root mean square error of prediction (RMSEP) for glucose and ethanol came out to be around 1.78% and 4.48% respectively.

The use of an HPLC for online monitoring of fermentation broth parameters has been studied and developed. Liu *et al*., (2001) developed a low cost, automated sampling system using Microsoft Visual Basic for monitoring and controlling of fermentation parameters. The automatic equipment (Bench Mate II) could perform the pipetting of a sample from the broth, filtration, dilution, and injection of the sample into the HPLC detector plate through the automated program in the Microsoft Visual Basic. This system was applied to the ethanol fermentation of *Zymomonas mobilis* model; and the glucose and ethanol were analyzed online using an automated sampler that was linked with HPLC and computer through the interface.

All the above-mentioned methods for the measurement of glucose and ethanol during fermentation involved either direct screening of the sugars or in-direct measurement of alcohols via monitoring carbon dioxide. Some direct screening methods involved the sampling technique, whereas, in others no sample preparation was required and real time monitoring was possible. However, all the methods monitored at most two fermentation reactors. They were not designed for the high throughput analysis of fermentation in real time. Our design sought to pass the carbon dioxide evolved during fermentation through an orifice to produce bubbles, and then to sense the bubbles optically. This design used a single web camera to monitor multiple fermentations in real time, and this approach did not

involve the collection of samples from the fermentation broth. To get effective bubble detection by the optical sensor, literature on bubble formation at a submerged orifice was reviewed.

Bubble Formation

A semi-empirical model based on the force balance under constant flow conditions for determining the bubble size during the detachment from the submerged nozzle was developed (Snabre and Magnifotcham, 1998). A glass tank of 20 x 20 cm cross section with 20 cm height was filled with a Newtonian water-glycerol solution with a viscosity in the range of 43 mPa s up to 800 mPa s, and density in the range from 1200 kg/m^3 to 1260 kg/m^3. The liquid temperature was maintained at 20 ℃ using a water jacket around the gl ass tank. A constant airflow rate up to 0.5 l/min was passed through a steel tube of 10 cm length with varying inner diameters of 0.3 mm, 0.4 mm and 0.6 mm. The submergence of the orifice in the Newtonian liquid was also varied in three levels, ranging from 5 cm to 12 cm from the bottom of the tank. The rising bubble stream was analyzed using a 512 x 512 pixel resolution CCD Sony camera (XC77RR) with 256 grey level resolution. Snabre and Magnifotcham, developed specific algorithms to determine the average bubble size and rising velocity with 2% accuracy in successive image frames. They also studied the effects of fluid viscosity, gas flow rate, orifice diameter, and liquid depth on the bubble stream dynamic. The results from their model showed that at low flow rate (Q< 0.02 l/min), surface tension plays a

dominating role in bubble formation, and the bubble diameter was very sensitive to the orifice diameter. However, at high flow rates, orifice diameter did not play a significant role in the bubble formation because either viscous force or inertial force was the dominating downward force.

Hayes *et al.,* (1959) studied the correlation between the physical variables of the orifice system and the bubble formation through the application of Newton's second law of motion during the bubble detachment at the orifice (Hayes *et al.,* 1959). The orifice system used in the experiments consisted of a column of 10" diameter and 72" high, an orifice holder of 2" diameter and 22" of length, six orifice plates of 0.318 cm thickness, with orifice diameters of 0.0794, 0.159, 0.238, 0.318, 0.397 and 0.635 cm. They studied the effect of gas chamber volume, gas flow rate and various effects of the apparatus dimensions on bubble formation. They also observed two types of bubble formation during their experiments. The first was that at low gas flow rates, the volume of the bubble remained constant, but the frequency of the formation was increased with increased gas flow rate. The second type was that at high flow rates, in which case the bubble formation frequency remained almost the same, but the bubble volume was increased with the increased gas flow rate. Moreover, they had also observed that the bubble formation was independent of the gas chamber volume when the gas chamber volume was greater than 800 cm^3. Also, they stated that at very low gas flow rates the bubble size was determined by the orifice diameter and surface tension forces.

Moreover, another study (Byakova *et al., 2005*), showed that the bubble formation at an orifice in water was affected by the hysteresis of the contact angle and the bubble volume increases with the increase in contact angle for both aqueous and metallic compounds. Bubble formation was tested at good wettability, where contact angle was between 68° and 90°, and at po or wettability for contact angle in the range of 90° to 110° (Byakova *et al*., 2005). The effect of orifice submergence on bubble formation was also studied and showed that beyond 25 cm there was a decrease in the bubble size (Iliadis *et al*., 2004). In the single bubble formation zone the bubble size increased with the submergence depth, whereas in the group zone it is independent of the submergence depth.

Considering the results from the existing fermentation monitoring methods (Varga *et al*., 2004; Eliana *et al*., 2007 ; Warriner *et al*., 2002; Gemeiner *et al*., 2002; Varma *et al*., 1999; Weimer *et al*., 2004; Gunta M. *et al*., 2004), a high-throughput fermentation screening method using relatively low cost sensors was proposed by Anex and Raman (2007). As stated previously, high throughput fermentation screening is an enabling technology that could help scientists to evaluate several biomass feedstocks and pretreatment methods rapidly and inexpensively. The goal of this study was to develop and test such a method using fermentation of simple sugars. A continuous way of monitoring CO_2 using an optical sensor which would sense CO_2 bubbles coming out of multiple fermentation reactors at a time was investigated.

CHAPTER 3
SINGLE ORIFICE CHAMBER

An apparatus for the estimation of ethanol via carbon dioxide evolved during fermentation was developed in a series of several stages. The different stages in the development of the real time ethanol monitoring system are discussed below.

3.1 Materials and Methods

3.1.1 Orifice chamber design

Initially, a single reactor chamber was designed and built using a 50 ml plastic test tube (Fig 1). For the initial phase, we did not conduct fermentation, but instead used 40 ml distilled water in the test tube as the surrogate fermentation media. A hole was drilled at the 35 ml level on the side of the test tube and was connected to a syringe pump (Hover apparatus Co., Model No 600-000) via plastic tubing of 1/16'' ID. This multi-gear syringe pump employed a 10 ml syringe connected with tubing (Tygon PVC tubing, 5554K42, ID 1/16'' and OD 1/8'') to the test tube. In the preliminary experiments, controlled airflow rates from the multi-gear syringe pump were used to test the primary design.

The second part of the single orifice design involved the construction of the submerged orifice. The estimated ethanol production in 24 hours was around

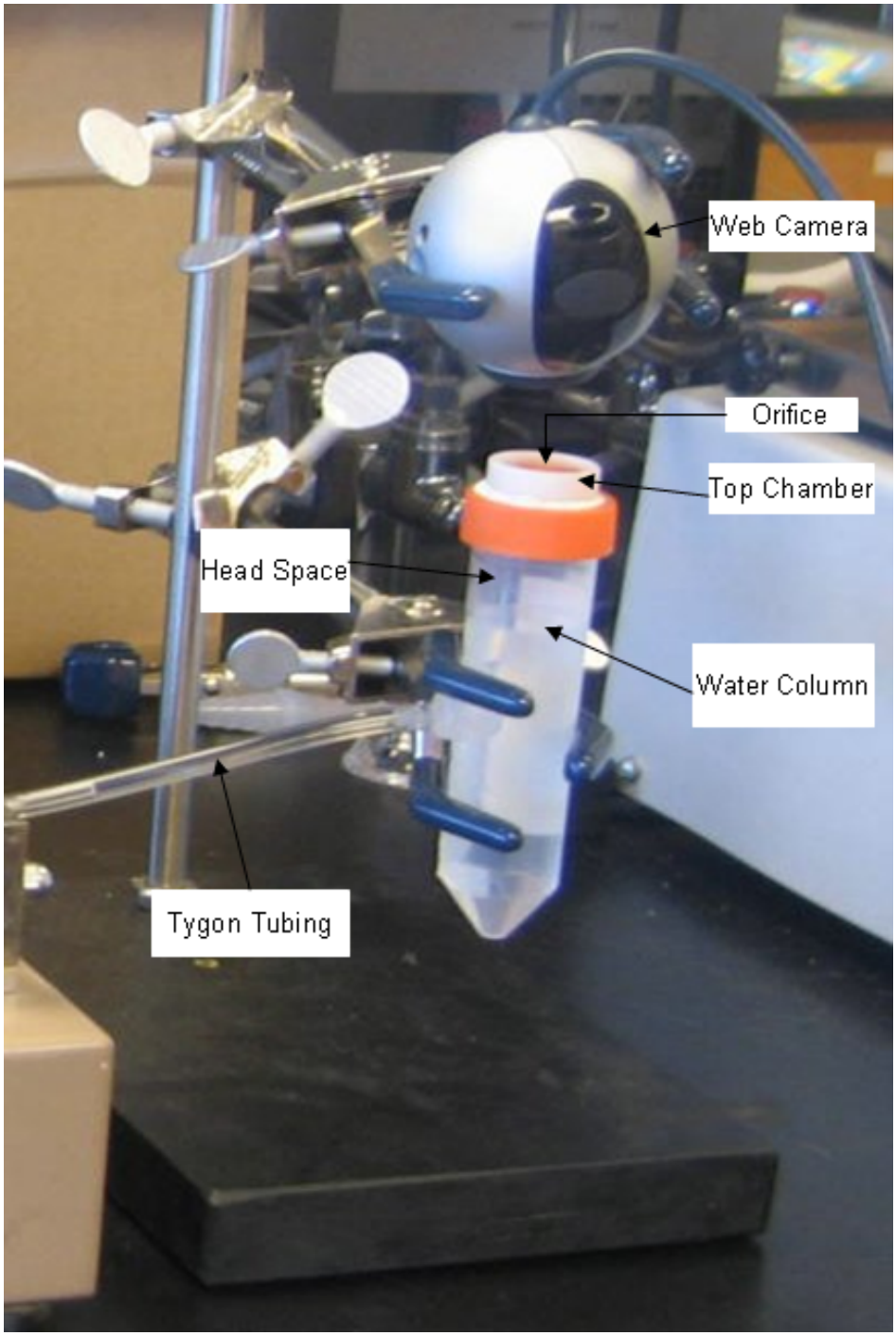

Fig 1. Single orifice chamber with orifice drilled into the orange color test tube cap.

0.8 g (20 mmol). In glucose fermentation, there is a one to one molar relation between ethanol and carbon dioxide evolved. At laboratory room temperature of 20 ℃ and pressure of 1 atm, one mole of an ideal gas has a volume of 24.04 L, so the average carbon dioxide production was estimated as 0.5 L/d, or 5.5 µL/ sec. The submerged orifice was designed targeting a single bubble per second at this average rate, thereby, making the target bubble volume 5.5 µL. For our study, we assumed the spherical bubbles at the time of detachment and thus the bubble diameter was calculated as 2.2 mm for bubble volume of 5.5 µL. The orifice diameter was calculated using the following equation (Perry and Chilton in 1973),

$D_b^3 = (6*D*\sigma) / [g*(\rho_l-\rho_g)]$

Where, D_b = Bubble diameter

D = orifice diameter

σ = Interfacial tension of gas liquid film, taken as 0.07 N/m

ρ_l = Density of liquid (for water,1000 kg/m^3)

ρ_g = Density of gas/CO_2 (1.799 kg/m^3)

resulting in an orifice diameter (D) of 0.256 mm.

However, for this experiment, the orifice diameter was chosen as 0.34 mm due to the limitation of the drill press used in the fabrication of the orifice. A back calculation was done using the above equation for the determination of bubble diameter for 0.34 mm orifice diameter, which yielded 2.64 mm as the bubble

diameter and 9.62 µL as the bubble volume. Because of the small diameter of the orifice drilled into the test tube cap, there was minimal leakage of water down through it. A 1 cm high, 2 cm diameter rim was placed around the orifice and was filled with water up to 1 cm height resulting in the submerged orifice (Fig 1). Liquid height above the orifice was kept twice the calculated bubble diameter, as then there would be no effect of height on the bubble formation as reported by Iliadis *et al*., (2000).

Several trials were conducted using different airflow rates, which were controlled by the syringe pump, and the bubbles were counted manually and through the Matlab (R2007a version) program, when the flow rate was 0.412 ml/min. For high flow rates, the bubbles were detected only by the web camera (Logitech quick cam IM, 1.3 megapixels, VGA sensor) which was interfaced with Matlab due to the human eye limitations in detecting fast bubble counts.

3.1.2 Image Analysis (Energy Method for single orifice chamber)

A data acquisition system was developed which consisted of a web camera and a Matlab program for determining the number of bubbles released during the fermentation. As the fermentation proceeded, carbon dioxide was evolved in the test tube and exited through the orifice in the cap and the liquid column above the orifice, which eventually resulted in the formation of CO_2 bubbles. These bubbles were then imaged by the camera placed directly above the test tube.

The initial version of the Matlab program operated on the basis of image energy changes by taking the summation of the absolute values of the current frame's pixels subtracted from the previous frame's pixels, so for differentiating the two versions of Matlab program, we named this version as the ‘’Energy Program.’’ When the web camera's view changed from frame to frame, the image energy changed. The frame-to-frame energy change was used to detect bubbles. The program was initiated by declaring the run number, pump position number, and number of tubes.

A region of interest (ROI) was selected in the image for each tube. For the single orifice chamber, the energy program was coded for a single test tube. Selecting a ROI minimized the effects of ambient light change, persistent surface bubbles, and other disturbances during the detection of emerging bubbles. The energy change in the ROI from frame to frame was then found by taking the summation of the absolute values of the current frame's pixels subtracted from the previous frame's pixels. A threshold determined by observing the test tube with no bubbles present was compared to the final energy change. A bubble was detected when the final energy change went above and returned below the threshold level. The camera was operated at 15 frames per second (due to limitation of the Matlab software to run at 30 fps) to ensure thorough resolution. Bubble detections were counted over five second intervals and output to a text file.

3.1.3 Experimental Design

This initial single orifice reactor chamber was tested at airflow rates from 0.412 ml/ min to 1.03 ml/min. The bubbles were counted both manually and with the energy program. The web camera was positioned 3 cm directly above the orifice and the initial trial was conducted at 0.41 ml/min and 1.03 ml/min (Fig 2). To get a stable pressure inside the chamber volume/head space, the energy program (single orifice chamber) was initiated after a few seconds delay from the pump initiation time; the bubbles were also counted manually. Four runs were made at each flow rate and the bubbles were detected by the energy program. Bubbles were also counted manually from the start of the energy program to the end of the run. At high flow rate, each run was for one minute and for low flow rate, the run time was 2 minutes (See Results and Discussion, Fig 3).

The single orifice system was also tested over six different controlled flow rates to check the functionality of the system at varied flow rates in the range around the flowrate assumed in the design. In this case, the web camera position was kept at the same height and four runs were made at each flowrate for one-minute duration. A simple statistical analysis was conducted over the data, and averages and standard deviations of the bubble count were computed for each of the flow rates (Table 2, Results and Discussion). Total bubble volume was computed by multiplying the bubble count with the theoretical bubble volume of 9.62 µL. The actual volume injected into the system and the bubble volume coming out of the system could thereby be compared. The calculated bubble volume

coming out of the system was very low compared to the injected volume for each of the six flow rates (See Results and Discussion, Fig 5).

To understand why there was such a difference between the input and calculated gas volumes, several other trials were also conducted for the determination of the bubble size after detachment. These were performed by recording the video using the Logitech quick cam IM software. The web camera was placed directly above the test tube cap in which the orifice was drilled, at a height of 3 cm above the orifice. A ruler was placed at 1 cm height above the orifice and its video was recorded for 1 minute. Then air was passed at 1.03 ml/min through the headspace using the syringe pump, and four bubble videos were recorded; two videos at 3.2 ml injected volume and the other two at 3 ml injected volume. The recorded bubble video was then played at ¼ speed in Window Media Player and was paused when there was emergence of bubble at the water surface. The bubble diameter was measured individually over the record time using the same ruler whose video was recorded, and the actual diameter was computed using the scale factor. The scale factor was calculated from the ruler video, which was played in the Window Media Player and 2 mm actual on the ruler was measured by scale on the computer screen as 15 mm (2mm on scale was 15 mm on video) so, the scale factor was 2/15 = 0.1333. Actual bubble diameters were close to each other (See Results and Discussion, Fig 6) and from the bubble diameter, bubble volume was computed individually. A comparison of the total bubble volume with the injected volume for each of the videos was done (See Results and Discussion, Fig 8).

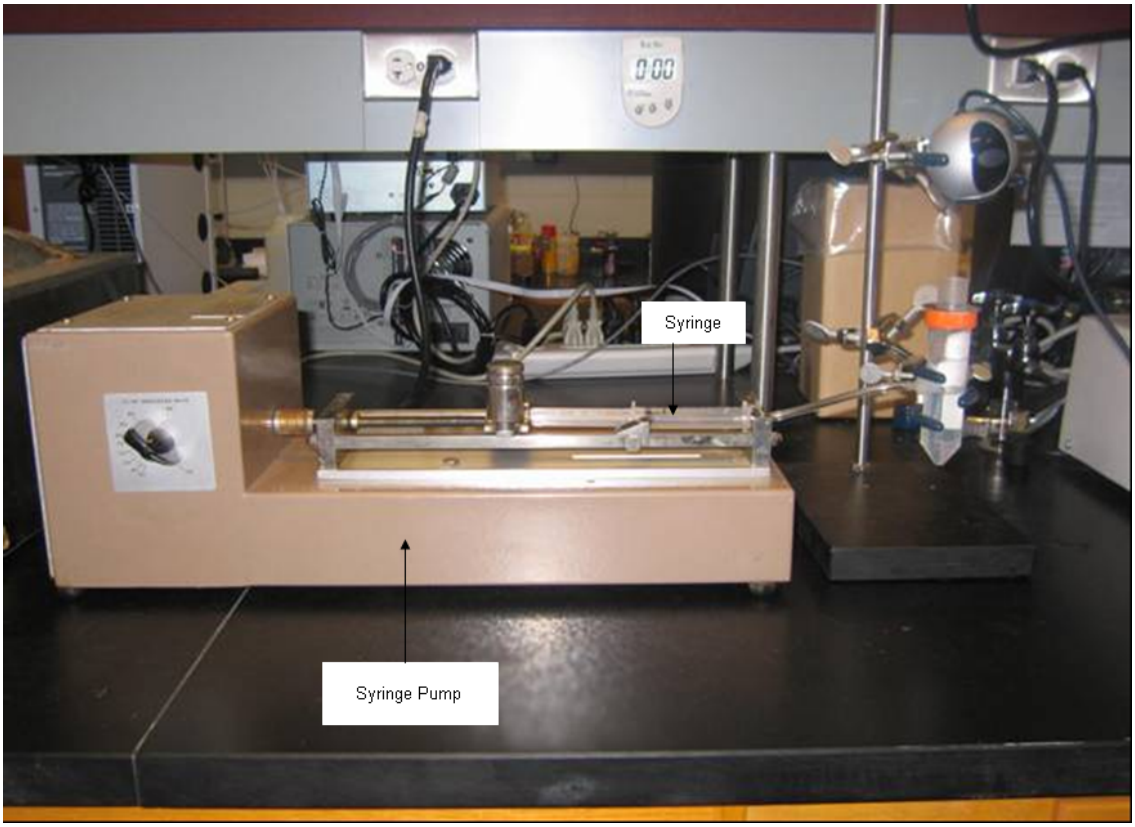

Fig 2. Single orifice chamber along with the syringe pump

3.2 Results and Discussion

For the initial single orifice design, air was used to test the orifice system and several experiments were conducted to characterize the performance of the system. The syringe pump was calibrated using a 10 ml disposable syringe and the data are shown below. It was observed that the flow rate values were one tenth of the flow rate settings provided on the pump. We believed that the pump nameplate was erroneous due to a modification in gearing made by a prior owner of this > 40 year old pump.

Table 1. Calibration data for the syringe pump

Pump gear position	Flow rate setting ml/min	Observed flow rate ml/min
1	10.3	1.03
2	4.12	0.41
3	2.06	0.20
4	1.03	0.10
5	0.51	0.05
6	0.20	0.02

After the calibration of the syringe pump, the single orifice chamber was tested at two pump controlled flow rates, gear positions 1 and 2 with four runs at each position. The energy program was used to count the bubble production at these two flow rates. The bubble count for two different flow rates, one at 1.03 ml/min and other at 0.41 ml/min over the one-minute run is shown in Figure 3.

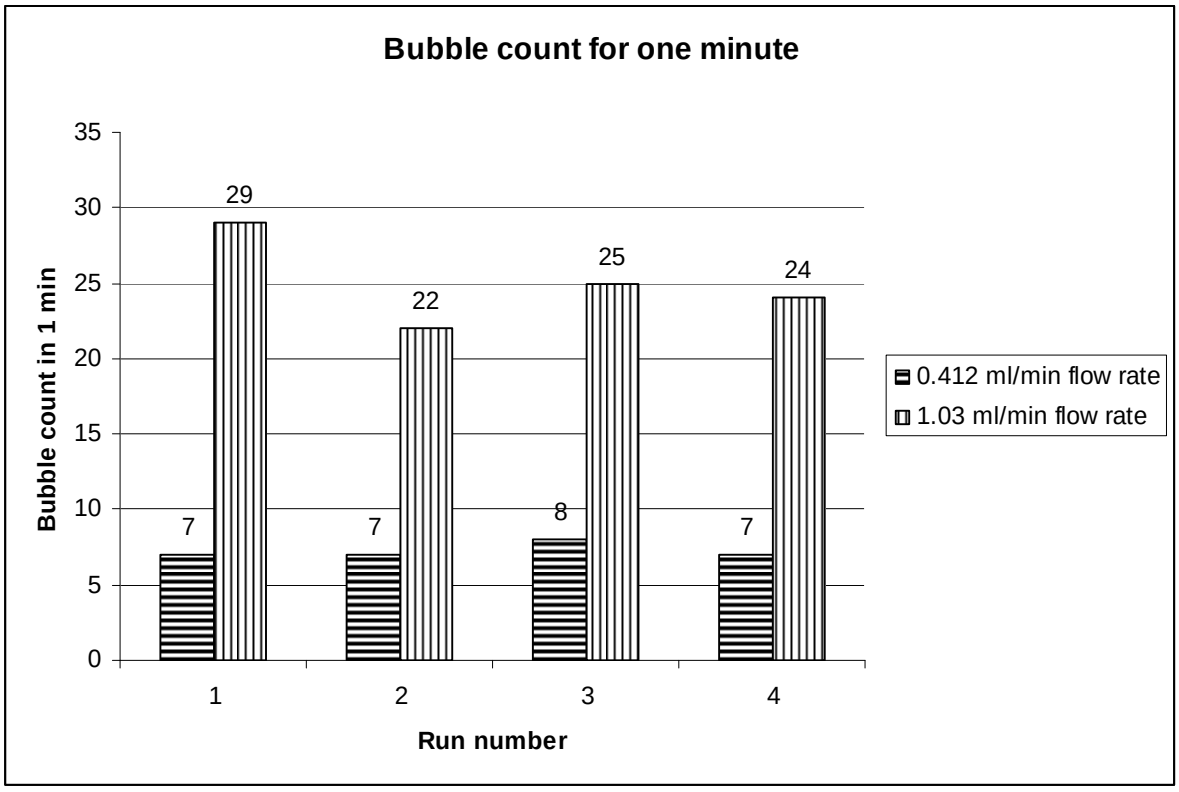

Fig 3. Total bubble count at 0.41 ml/min and 1.03 ml/min airflow rate for four runs respectively for a one minute run through the single orifice.

The total number of bubbles counted at 0.41 ml/min showed good consistency in the bubble count for a one-minute run. Good consistency in the count could also be attributed to the fact that at low flow rates, bubble formation falls in the single bubble formation zone, that is, they occur one by one as reported by Iliadis *et al*., (2004). Also, the single orifice chamber was designed for the flow rate close enough to 0.41 ml/min. However, taking the theoretical bubble volume of 9.62µL, the total volume for 7 bubbles was 0.067 ml, only 16 % of the 0.41 ml injected. At a flowrate of 1.03 ml/min, there was more variation in the bubble count. This could be due to the fact that at high flow rate, pressure inside the chamber volume/headspace fluctuated, which in turn effected the bubble eruptions. The pressure fluctuation inside the chamber volume has an effect over the bubble size and the bubble emergence frequency (Hayes *et al.*, 1959). The total estimated bubble volume was 0.24 ml, which was 23% of the injected volume for one minute – a slightly higher percentage than for the lower flow case.

A further probe into this matter was done by recording the bubble count using the energy program at six different flow rates ranging from 0.41 ml/min to 1.03 ml/min for a total run time of one minute. Table 2 shows the average bubble count for four replications at six flow rates and the average bubble volume which was computed by multiplying the bubble count with the theoretical volume of a single bubble, i.e. 9.78 µL. A graph of the flow rate and the bubble count for four runs was plotted (Fig 4). From the data in Table 2, there was an inference that as the flow rate was reducing, the standard deviation was decreasing, but there was an

outlier in this data at the flow rate of 0.618 ml/min with a standard deviation of 3.56. We had expected the standard deviation for the bubble count to be low or nearly zero, in order to have a robust orifice chamber that could produce consistent bubble count for a known flow rate. Out of six flow rates, we measured consistent bubble count at the flow rate of 0.41 ml/min, which was the minimum flow rate used in getting these data. To have a clear picture, a graph between the total bubble volume versus flow rate was also plotted (Fig 5). A linear equation fit well on the total bubble count and bubble volume data points with R^2= 0.91 for both the data plots. However, the total bubble volume at individual flow rate did not match the flow volume injected into the system. We expected that the constant value in the linear equation to be 1.0 instead of 0.27 and the intercept to be zero instead of -0.038 (Fig 5). Ideally, we wanted the bubble volume from the orifice system to fall on the diagonal line with slope of one, but we got the results falling on line with slope 0.27. Moreover, in this experiment the percentage of bubble volume for flow rates of 0.41 ml/min and 1.03 ml/min was the same as in the previous experiment. It showed that the bubble count as well as bubble volume for these two flow rates was consistent but still not acceptable. The 3.6 factor difference between the theoretical and experimental volumes shows average bubble volume would have to be 35 µL, corresponding to bubble diameter of > 4 mm, but we did not observe bubbles this large. Some underprediction could be due to ineffective sensing and illumination. For example, missed bubbles by the energy program would lead to reduce bubble counts. Also, air diffusion through the bubble film may be responsible for some of the size difference.

Table 2. Average bubble count and volume for six flow rates for one min run for single orifice chamber

Flow rate ml/min	Mean bubble count	STDEV	Estimated Average Volume (ml) *	Estimated volume/ true volume %
1.03	25	2.94	0.241	23
0.87	21	1.50	0.200	23
0.77	19	1.29	0.178	23
0.61	13	3.56	0.125	20
0.51	11	0.82	0.106	21
0.41	7	0.50	0.070	17

Note: Average Volume ml * was based upon the theoretical bubble volume of 9.62 µl.

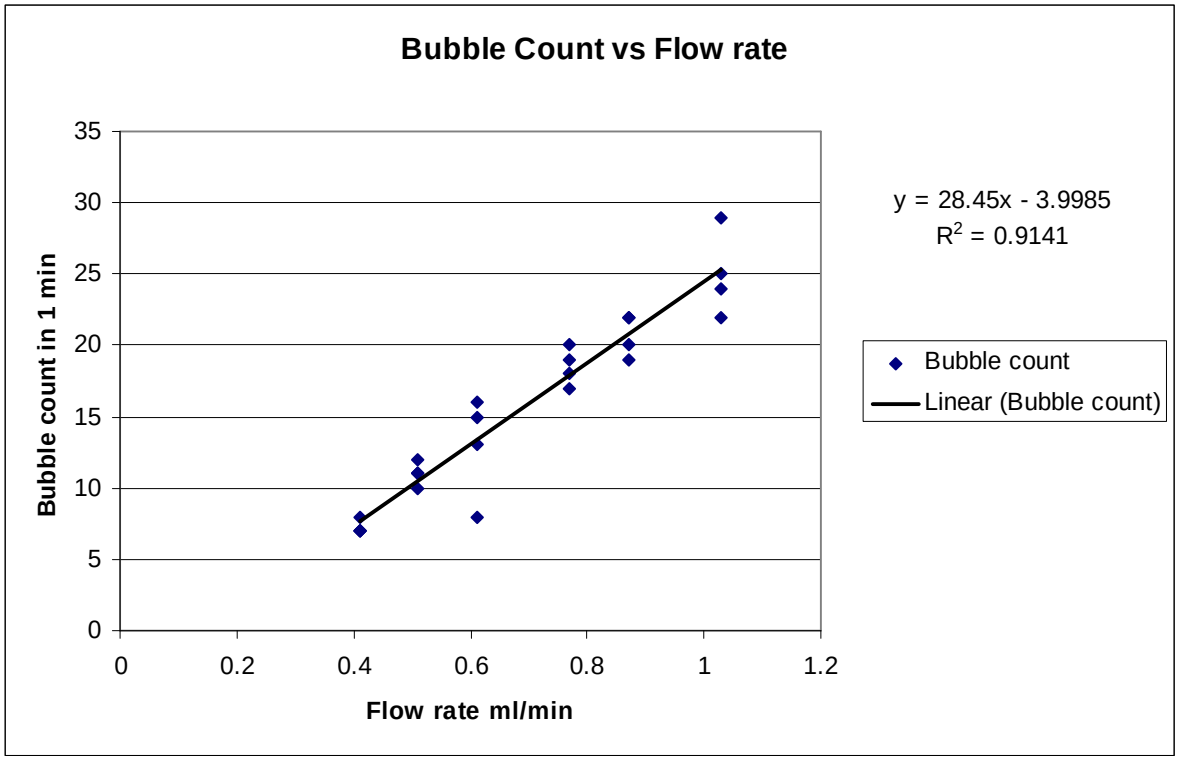

Fig 4. Bubble count for one minute at six controlled air flow rates for single orifice chamber for four runs at each flow rate.

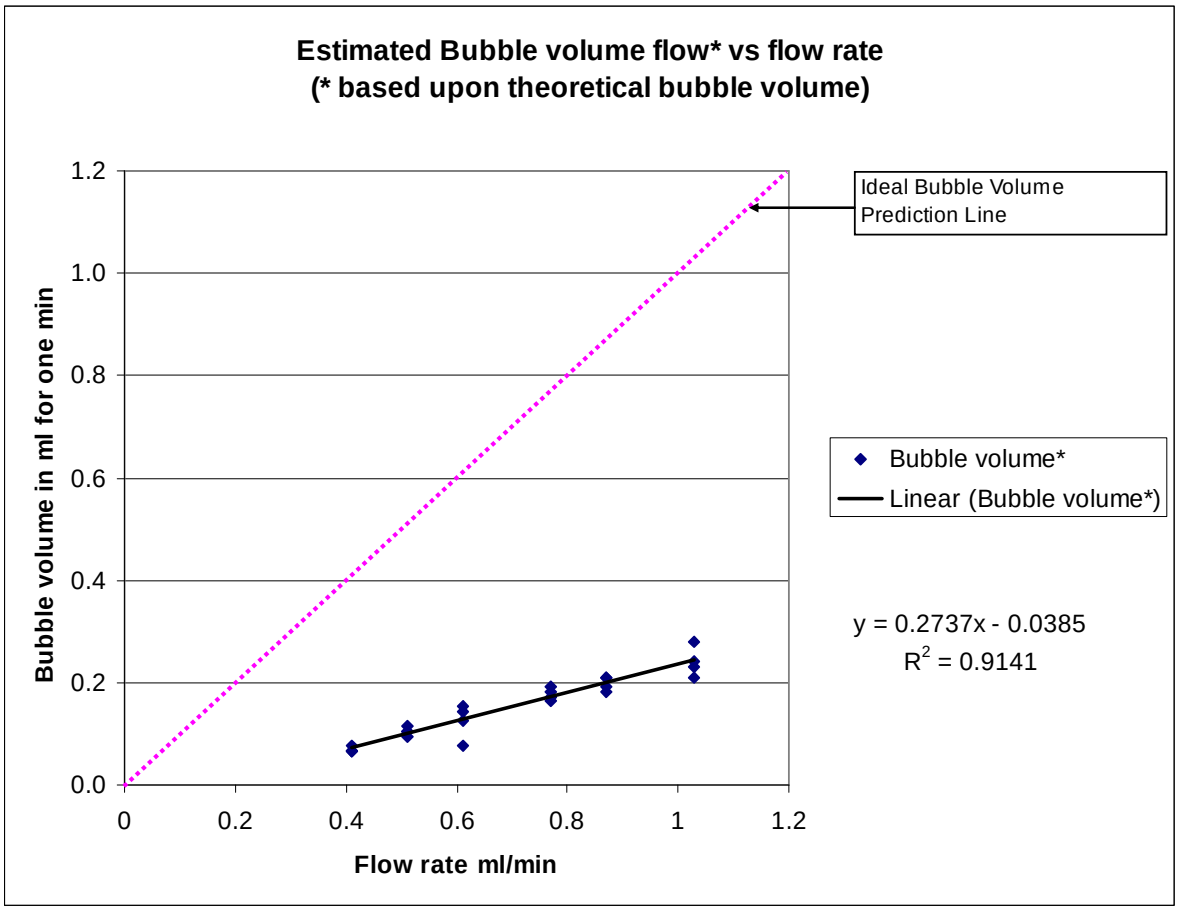

Fig 5. Bubble volume in ml for one minute run at six controlled air flow rates for single orifice chamber for four runs at each flow rate.

An uncertainty analysis of bubble diameter was done. To do so, the uncertainty in each of the following variables was estimated and reported below.

Table 3. Estimated Uncertainty value for orifice diameter, surface tension and density

Variable	**Estimated error**	**Rationale**
Orifice Diameter (D)	± 10%	Plastic material
Surface Tension (s)	± 1.4%	Based on variation in surface tension with temperature
Density Difference (ρ)	± 0.03%	Based on variation in density difference density with temperature

Using the following equation, the uncertainty in the bubble diameter (σ_{Db}) was calculated as ± 3%.

$$D_b = f(D, s, \rho)$$

$$\sigma^2_{D_b} = \left(\frac{\partial f}{\partial D} * \sigma_D\right)^2 + \left(\frac{\partial f}{\partial s} * \sigma_s\right)^2 + \left(\frac{\partial f}{\partial \rho} * \sigma_\rho\right)^2$$

But the observed bubble size variation was larger than the calculated uncertainty. For the computation of the uncertainty, we had assumed the dependence of bubble diameter over orifice diameter, surface tension and density difference of the liquid and gas phase as from the equation by Perry and Chilton,

1973. This equation was suitable for single bubble formation under low-flow conditions, and the cause for high variation than computed may be attributed to the group bubble formation observed during the experiments.

Looking at the volume variation with the ideal case and experimental results from Fig 5, further experiments were conducted to check the bubble size consistency for the single orifice chamber. This was done by passing the air at controlled flow rate through the orifice chamber using the syringe pump and recording bubble videos at different flow rates, with the web camera at a height of 3 cm above the orifice. The recorded videos were run at one-quarter speed in the Windows Media Player, and then the bubble diameter was determined by applying the scale factor of 0.1333. The data showed a moderately consistent bubble size, though some variations in the sizes were observed at the same flow rate for four runs (Fig 6). The single orifice chamber was run at the same flow rate to measure the bubble diameter using the scale factor, but the data showed less variation in the true bubble sizes, ranging from 2.48 to 3.24 mm. The theoretical bubble diameter was 2.64 mm and from Fig 6, it shows that out of four runs, bubble diameter from the three runs were close to the theoretical bubble diameter value. Now, from the measured bubble diameter, bubble volume was computed for each bubble and the total bubble volume was summed up over the count for each video. Fig 8 shows the total measured bubble volume with respect to the injected volume. The total bubble volume falls in the range of 39% - 55 % of the injected volume for this data set. Still the reason to why there was difference in the bubble volume and the injected

volume is not clear. This difference can be attributed to leakage of air from the syringe, tygon tubing and the connector attached to the test tube. Leakage from the syringe and the whole apparatus was checked by an air-water displacement method and the results showed that there was non-detectable leakage from the syringe.

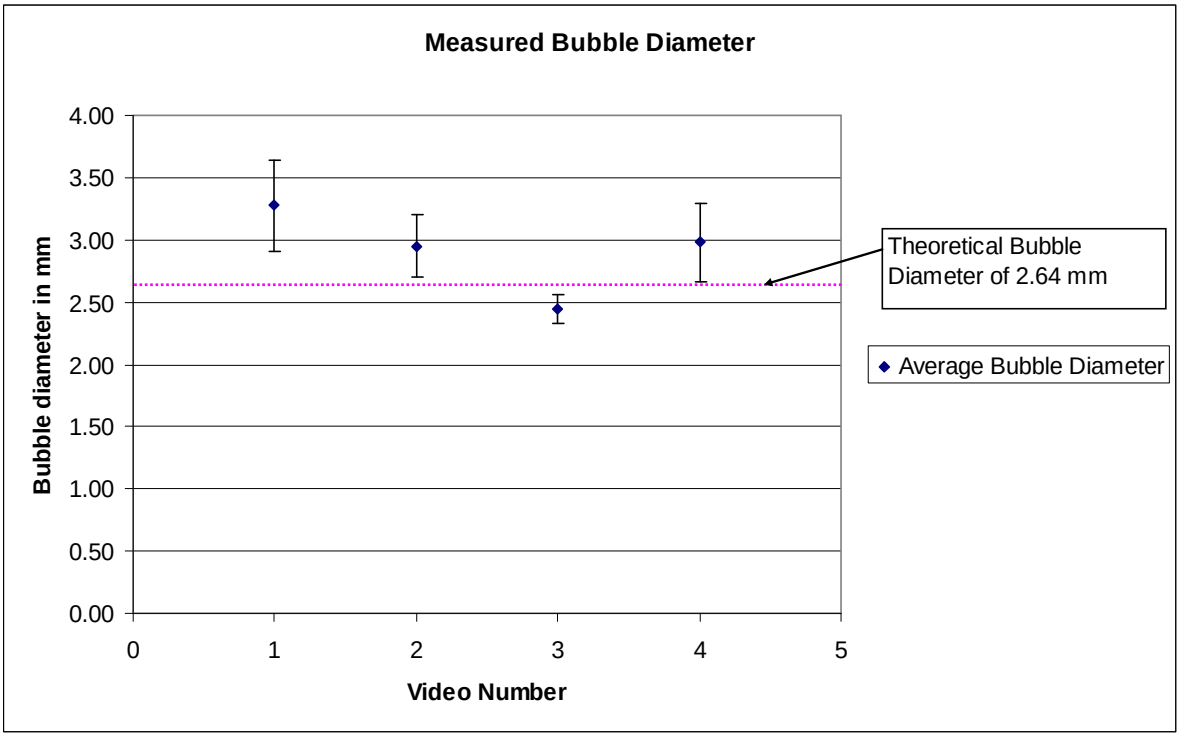

Fig 6. Average bubble diameter in mm for four videos at flow rate of 1.03 ml/min for single orifice chamber using a ruler to measure the diameter.

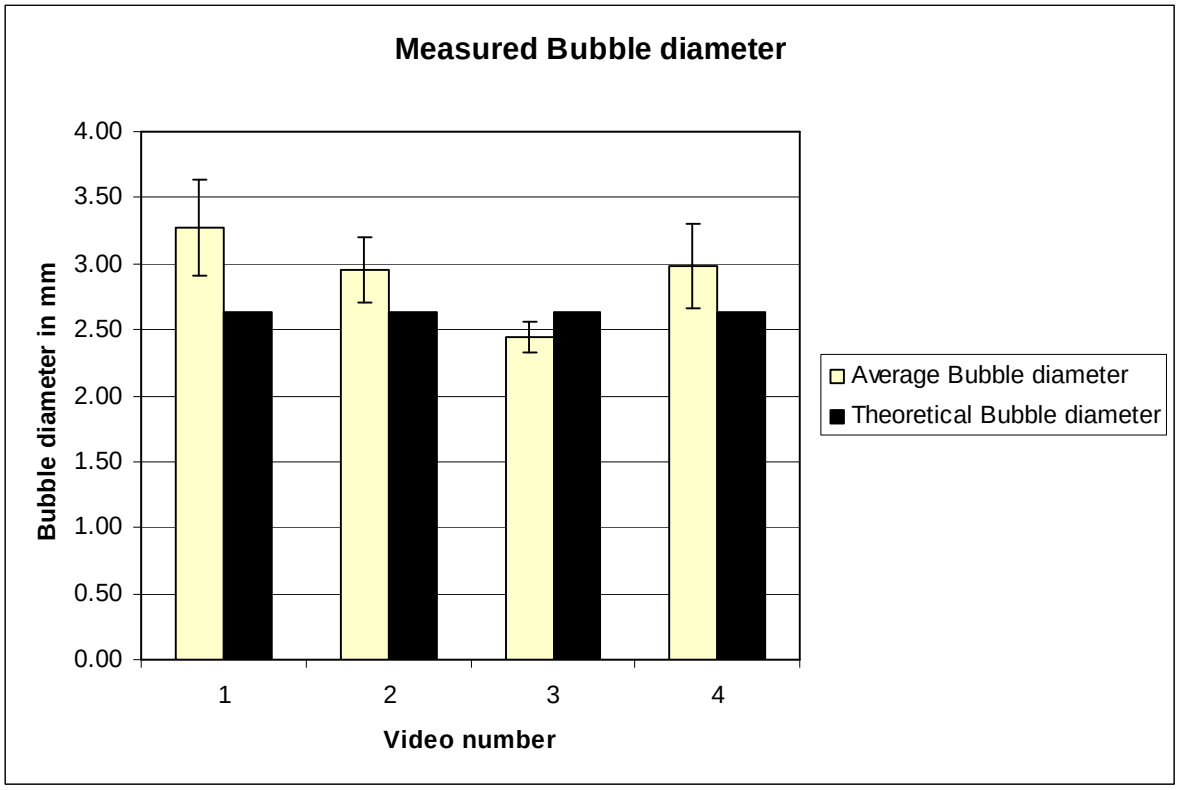

Fig 7. Measured bubble diameter along with the theoretical bubble diameter of 2.64 mm for four videos at flow rate of 1.03 ml/min for single orifice chamber.

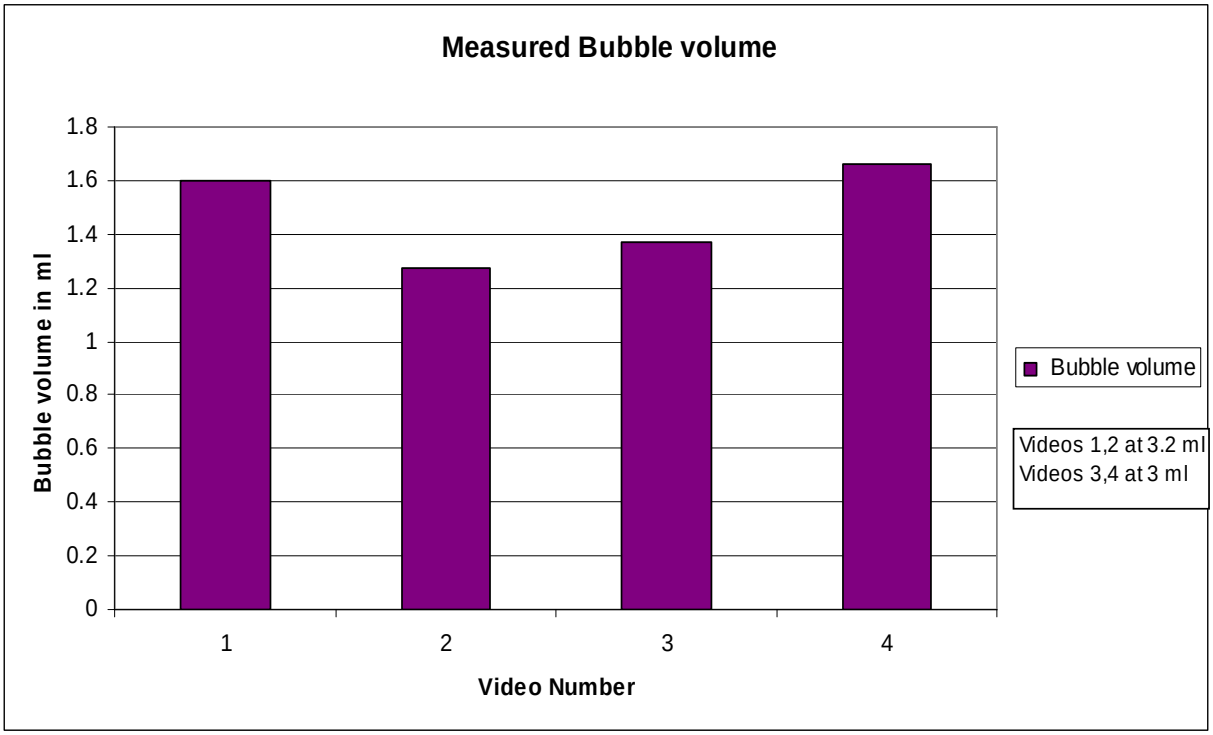

Fig 8. Bubble volume in ml from measured bubble diameter of individual bubble using ruler for four videos.

CHAPTER 4

MULTI ORIFICE CHAMBER

4.1 Materials and Methods

4.1.1 Eight-orifice chamber design

The promising results from the single orifice system (e.g. Fig 5) encouraged the development of a multi-orifice system for further testing. An eight-orifice chamber was designed on the same design basis as that for the single orifice chamber. All the eight 0.34 mm diameter orifices centered on 1 cm deep, 2.8 cm diameter wells were machined into a 20.3 cm x 12.6 cm x 2.0 cm (L x W x D) aluminum plate. The holes were placed in two rows with 4 orifices in a row having 4 cm distance between orifices (Fig 9 and Fig 10). Erlynmeyer flasks (50 ml) with 40 ml working volumes were used for the fermentation of simple sugars. Fermentation was performed at 35 ℃ in a water bath shaker at 155 rpm (New Brunswick Scientific Classic series, C76 water bath shaker, Edison, NJ, USA). In order to minimize the effect of disturbances caused by water bath shaker in the detection of bubbles through the web camera, the aluminum plate was held separately outside the water bath shaker and the fermentation flasks were kept inside the shaker. The flasks were connected with the plate using threaded connectors and the Tygon tubing of 1/16'' ID (Fig 11).

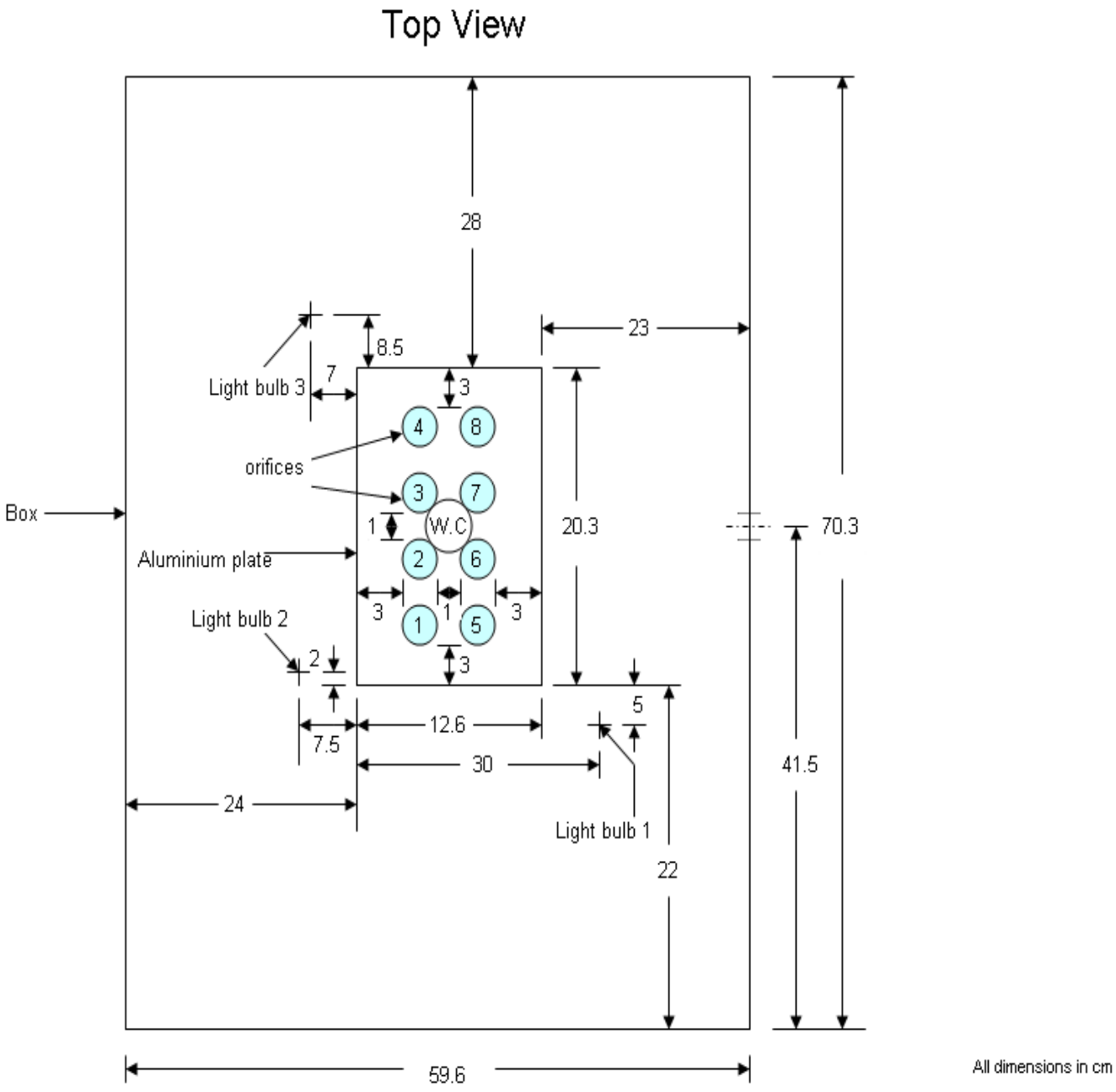

Fig 9. Top view of the eight-orifice plate with the three desk lamp positions

Note: W.C. is the web camera

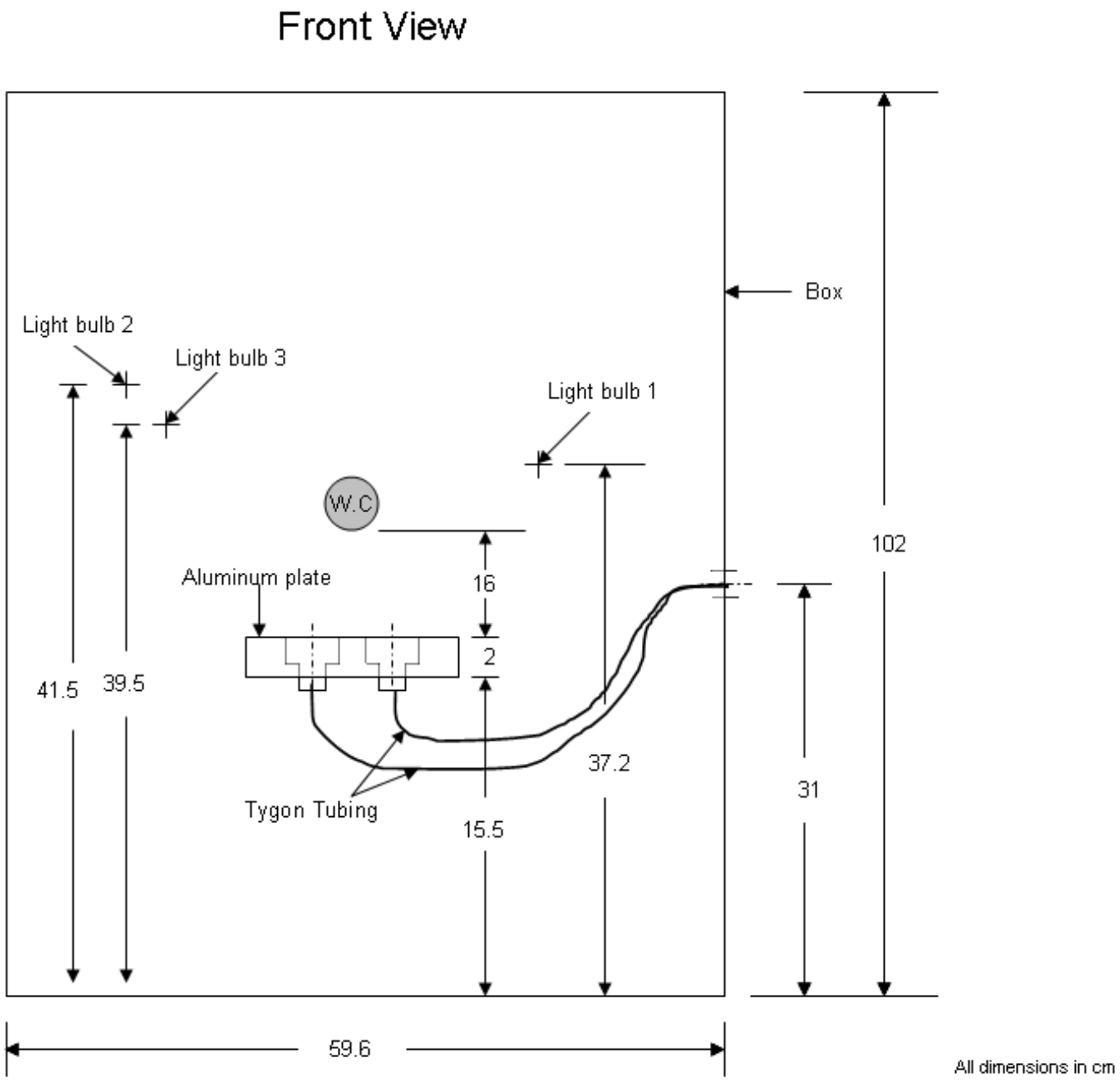

Fig 10. Front view of the eight-orifice chamber enclosed in the black box

Note: W.C. is the web camera

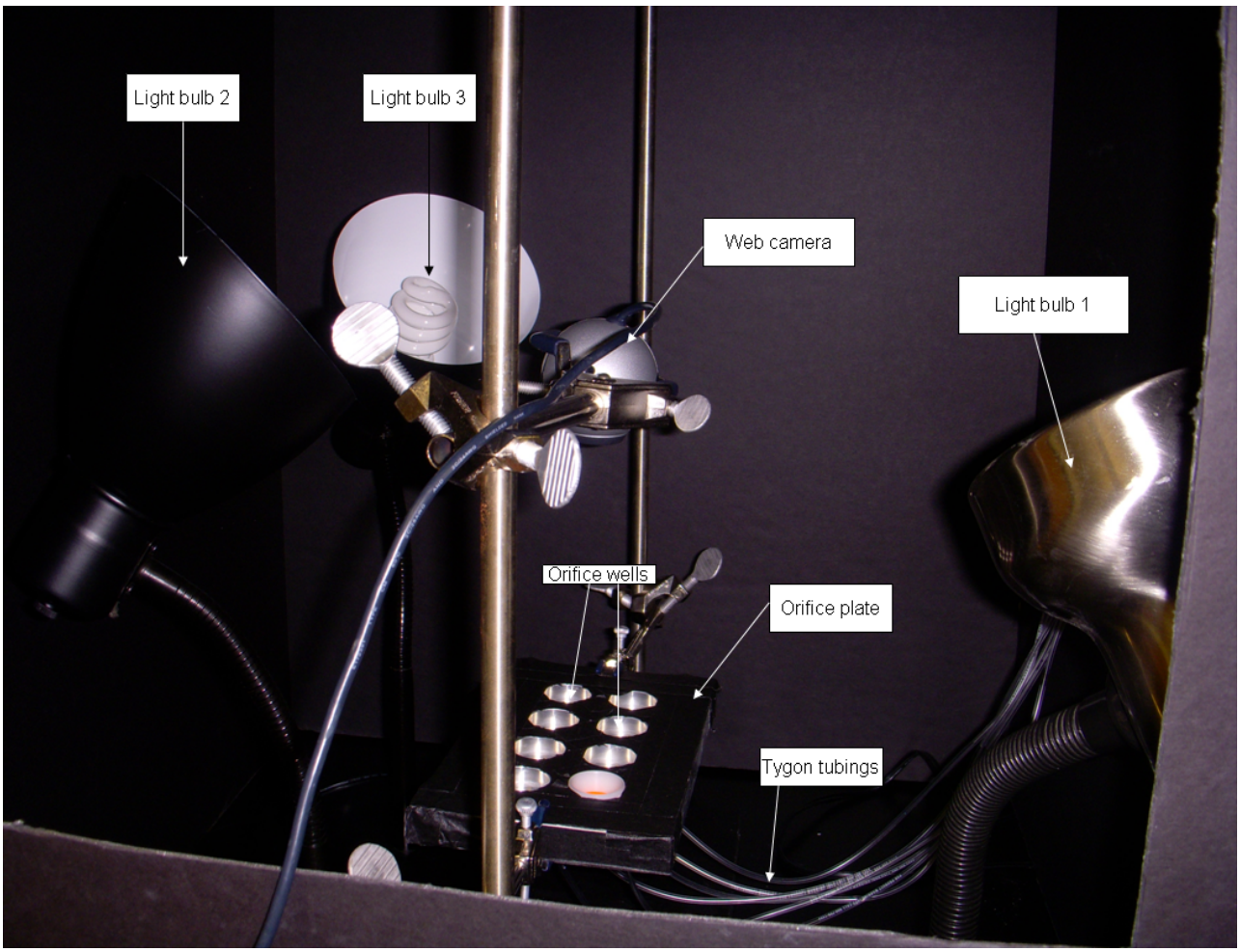

Fig 11. Orifice set up with three light sources enclosed in a black colored box

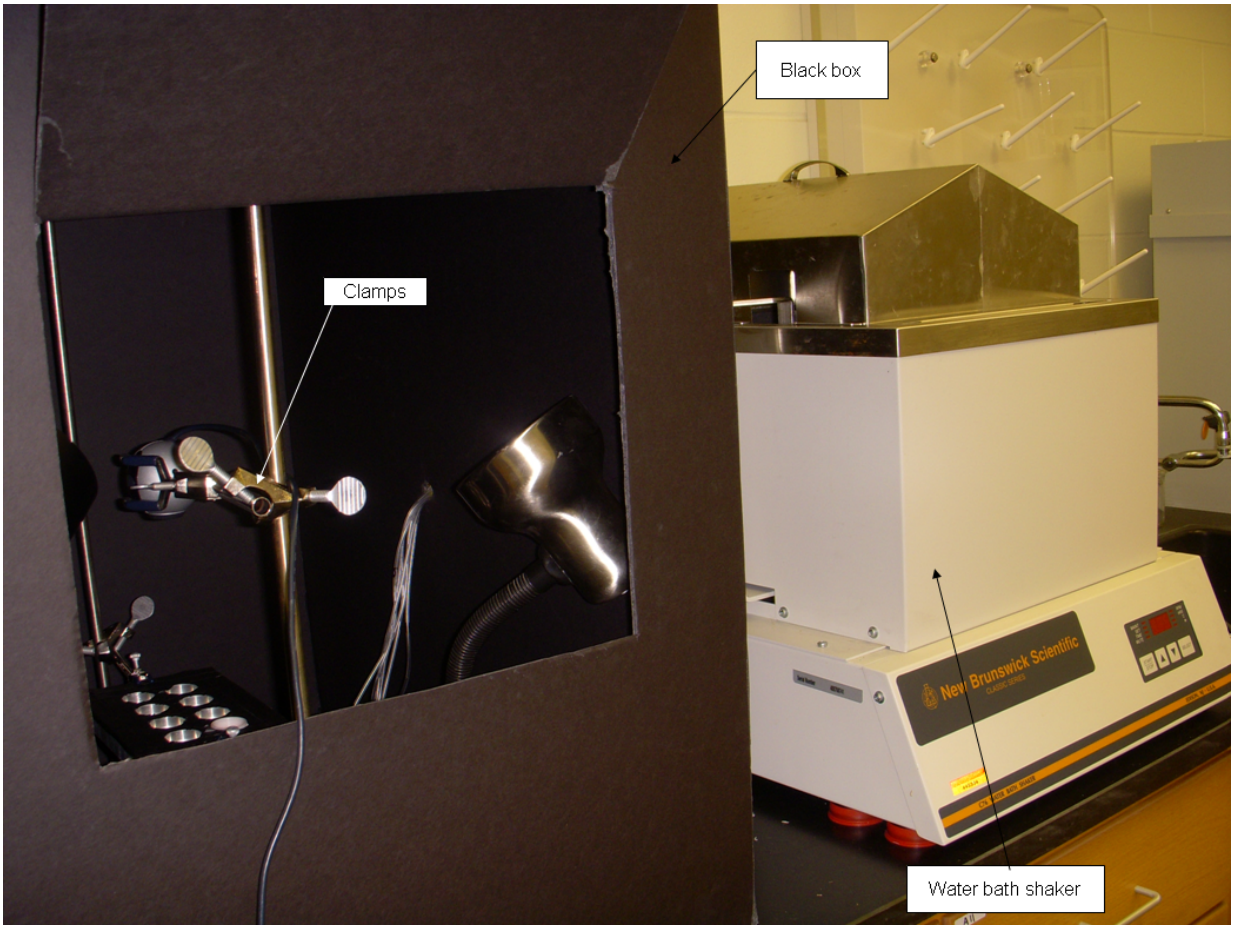

Fig 12. Orifice set up along with the water bath shaker.

4.1.2 Fermentation media

For the preparation of media, 0.75 g of glucose (Dextrose Molecular Biological Grade Anhydrous, BP 350-1, Fisher Chemicals, Fair Lawn, New Jersey), 0.8 g of peptone (Bacto™ Peptone, Enzymatic Digest of proteins, Becton Dickinson and Company, Sparks, MD, USA), 0.4 g of yeast extract (Bacto™ Yeast Extract, Extract of Autolysed yeast cells, Becton Dickinson and Company, Sparks, MD, USA) and 2 ml of 1.0 M citrate buffer of 4.5 pH were mixed with 36.05 ml of DI water to get 40 ml of fermentation media. The citrate buffer was prepared from 210 g of citric acid monohydrate (Fisher Chemicals, fair lawn, NJ), 750 ml of DI water and 50 g to 60 g NaOH (NaOH solid, UN 1823, Fisher Chemicals, Fair Lawn, NJ) until pH equals 4.5 (NREL Biofuels Program, Biomass Analysis Technology team, Laboratory Analytical Procedure, LAP-008). To this media, 0.22 g of baker's yeast (Red star quick rise yeast) was added instead of distilled dried yeast for all the testing experiments of the bubble chamber.

4.1.3 Analytical methods

The fermentation was carried in the water bath shaker at 35 ℃ and 155 rpm for 4 hours, and the samples were taken after 4 hours of fermentation for the determination of alcohol using the HPLC. The web camera was positioned at a height of 16 cm directly above the aluminum plate, centered on the length and width of the plate. The energy program (eight chambers) was initiated after the addition of

yeast into the fermentation flasks and the bubble count for 4 hours was stored in a text file, which was then imported in an Excel file. In the Excel file, bubble counts were shown over 5 second intervals throughout the run period. Total bubble count was computed by summing up the bubble count over 5 second intervals and the total volume of carbon dioxide produced was calculated by multiplying the total bubble produced with the theoretical bubble volume. As there is a one to one relationship between ethanol and carbon dioxide on a molar basis, the volume of carbon dioxide was converted into moles and then estimated production of ethanol was computed, which was then compared with the ethanol calculated from HPLC.

The HPLC system consisted of an ethanol column (Bio Rad column, Bio Rad laboratories, 2000, Alfred Nobel Drive, Hercules, CA); mobile phase of 0.01N sulfuric acid at a flow rate of 0.6 ml/min, auto sampler (Model 400, Varian), column oven (Prostar, Model 510, Varian) and refractive index (RI) detector (Prostar 355, Varian). Ethanol standards of 2.5, 5, 10, 20 and 30 g/l were used for the HPLC calibration based on peak area. Duplicate samples from each fermentation flask were taken after 4 hours of fermentation, so there were 16 samples from one run. These samples were analyzed for ethanol content through HPLC and the average ethanol peak area for each flask was obtained from the histogram computed in the HPLC. Ethanol concentration in g/l was computed from the calibration equation $Y = 5394*x$.

4.1.4 Energy method approach

The energy program for the single orifice chamber was expanded on the same conditions for the bubble detection for eight-orifice chamber. In this program, the number of test tubes/ROI was expanded to eight, which corresponded to the eight fermentation flasks and as well as eight orifices. In this case, the program was initiated by selecting the run number, and selecting the number of test tubes involved. The ROI for each test tube was selected individually and then the program was initiated to detect the bubble count. The energy change in the ROI from frame to frame was then found by taking the summation of the absolute values of the current frame's pixels subtracted from the previous frame's pixels. A threshold was set by observing the test tube with no bubbles present was compared to the final energy change. A bubble was detected when the final energy change went above and returned below the threshold level. Bubble counts were recorded over 5 second intervals for each of the eight orifices to be stored in a text file, which was then formatted in Excel.

The initial experiments were based on the fermentation media as mentioned earlier, for the testing of the eight-orifice chamber reactor and the energy program. The same media concentration was used to reduce any false positive readings in the bubble count and to rectify the energy program to the best possible level in order to have minimum error from ambient disturbances. After 4 hours of fermentation samples were taken in duplicates from each flask. These samples were centrifuged in 2ml micro centrifuge tubes (Polypropylene Graduated tubes with

locking lid, Fisher Scientific, USA) for 10 minutes at 6580 g in a Mini Spin plus centrifuge (Eppendorf) to separate the yeast from the media in order to stop further conversion of glucose into ethanol. After centrifugation, the samples were filtered through 0.2 µm nylon filter (Fisher brand, USA) and stored in 2 ml screw top clear vials (12*32 mm Clear vials with Septa inserted in cap, Varian, USA) at -20 ℃ in the freezer. The frozen samples were allowed to reach room temperature to be run on HPLC. Then these samples were analyzed through the HPLC for the determination of actual ethanol production. Actual ethanol estimation using the HPLC was then reported in terms of moles of ethanol produced. The total carbon dioxide bubble volume computed from the energy program was then converted on a molar basis for the comparison with the HPLC results. One mole of an ideal gas at laboratory room temperature of 20 ℃ and atmospheric pressure of 1 atm is equal to 24.04 L, so moles of carbon dioxide were calculated from it, which was compared to the moles of ethanol determination from the energy program.

After several initial trials with the same fermentation media to check the functioning of the orifice plate and energy program, the eight-orifice chamber was tested with fermentations at several glucose and baker's yeast levels. Four glucose levels of 0.3 g, 0.6 g, 0.9 g and 1.4 g; and 3 yeast levels of 0.1 g, 0.2 g and 0.4 g were selected, keeping peptone, yeast extract and citrate buffer level the same as in previous experiments, but DI water volume was changed according to the glucose and yeast level making the end fermentation volume of 40 ml. Table 4 shows the different sets of glucose and yeast.

Table 4. Twelve treatment sets with 4 glucose levels and 3 yeast levels.

Yeast / Glucose	0.1 g	0.2 g	0.4 g
0.3 g	A	B	C
0.6 g	D	E	F
0.9 g	G	H	I
1.4 g	J	K	L

So, there were 12 sets which were used to test the eight-orifice chamber but only 8 sets were selected to test the performance of the orifice chamber with the energy program (eight chambers), at the low and high yeast level. For each set, four replications were made and so, in one experiment two sets were involved as we had only eight orifices to connect with eight flasks. Firstly, set A and D were

selected and four replications were made for each set and yeast was not added to it. These eight fermentation flasks were then autoclaved for 20 min at 121℃. After the media was autoclaved yeast was added according to the amount mentioned for each set. The fermentation flasks were placed in the water bath shaker at 35 ℃ and 155 rpm. The flasks and orifice plate were then connected using the Tygon tubing via threaded connectors and water was filled up to 1 cm above the orifice in the orifice plate. The web camera was placed directly above the center of the aluminum/orifice sheet at a height of 16 cm and then the energy program was initiated. After 4 hours of fermentation, two samples were taken from each flask in the centrifuge vials. These samples were then centrifuged at 6580 g for 10 minutes in order to separate yeast from the media, and then the liquid media was filtered through 0.2 µm sterile filter paper which was then stored in 2 ml vials (Screw top 2 ml, 12*32mm vial with septa inserted in the cap) at -20 ℃ in the freezer. Similarly, sets G and J, C and F, L and I were done like sets A and D.

Changes in the glucose level would alter the ethanol level, so this would help in determining the functionality of the orifice chamber over a wide range of carbon dioxide pressure. On the same basis, yeast level was also changed from 0.1 g with increment of 0.1 g till 1 g. In all the experiments, working volume was 40 ml with the same peptone, citrate buffer and the yeast extract loading as used for initial testing. Each time samples were taken after 4 hours of fermentation to run in the HPLC, and then the actual ethanol production was compared with the energy program result. The results from the eight treatment sets showed that mol of ethanol

computed from the energy program were low as compared from the HPLC data (data shown in the Results and Discussion, Table 5).

A further analysis of the eight-orifice chamber was made at four controlled airflow rates using the syringe pump. A 10-ml syringe was used in the pump and was connected to the orifice plate via amber tubing. The orifice chamber was designed on the basis 5.8 µL/ sec flow rate and the performance of this system was then tested for a flow range from 0.10 ml/min to 1.03 ml/min. In this case, one orifice was connected with the syringe pump at a time. So, at each flow rate all eight orifices were run individually to get the bubble count. Before starting the pump, the energy program (eight chambers) interface was activated and then the region of interest was selected according to the orifice in connection with the pump. Then the syringe pump was started before initiating the energy program to avoid problems with the transient flows. The program was started after one minute and for each of the runs at four different flow position, 2 ml of air volume was passed through the orifice chamber and bubbles were counted manually and through the energy program. Bubble data for manual and program counts are presented in the Results and Discussion section (Table 10 and 11). Simple statistical analysis was applied to the data set.

For accurate measurement of the bubble volume we need to know the bubble diameter accurately. To determine the bubble diameter a new image analysis technique was developed. Initially, a still image of the orifice plate with a bubble was taken, and several edge analyses were applied over the bubble image.

One way of determining the diameter was to detect the bubble edge, and then to have an algorithm which could yield bubble diameter.

In order to have an effective detection of the bubble edge, a high contrast between the bubble and the aluminum plate was desired. This was accomplished by providing sufficient ambient light using 3 desk lamps. Moreover, the whole apparatus was enclosed in a black box made from foam board with a white top surface to reduce the ambient light shading effect on the orifice plate. The top surface was made white for the effective scattering of the light inside the black box as the desk lamps were positioned at an angle towards the top surface. The lights were placed in such a manner that whole orifice plate was well illuminated to get a good bubble video. The top surface of the orifice plate was then covered with black paper leaving the wells as bare aluminum to reduce the glare and color saturation (Fig 9 and Fig 10). While working to get a good contrast of the bubble image with respect to the surroundings, we rejected orifice 1 and 5, which were at the extreme left of the plate due to poor image contrast. So, for further work, we were left with only six orifices.

4.1.5 Shape Method approach

A new program was written for each of the eight orifices separately using the edge analysis and incorporating the horizontal and vertical cross hairs to scan the region of interest around the orifice. A region of interest of 40*40 pixels area was selected to reduce chance that ambient disturbances would lead to false bubble detections. The region of interest was fixed for each of the orifices in the code itself.

This area was selected such that when there was an emergence of the bubble from the orifice, only one bubble comes in that region to the best of our assumption. In this case, the web camera was positioned at a height of 16 cm as in previous experiments and directly above the middle portion of the plate being equidistant from width of the plate. The shutter speed was set at 0.015 s and the capture mode was set at black and white in contrast to the setting for the previous experiments on single and eight-orifice chambers with the energy program. This program worked on the recorded video and in the code for each orifice, the video number was changed accordingly to get the bubble detections. In this program also, the bubble detections and diameters were stored in a text file for each of the six orifices. This initial version of the shape program was written to process one orifice at a time in contrast to the energy program that could process eight orifices simultaneously.

Several calibration experiments were conducted with each of the six orifices to determine the effectiveness of the new shape detection program. Calibration of the shape program and the new version of the orifice set up were done using the syringe pump at the flow rate of 0.41 ml/min for each orifice. One orifice at a time was connected with the syringe pump via tygon tubing to the 10-ml glass syringe. The web camera was placed at the same position as in the previous experiments and bubble video was recorded for each of the five sets of 4 ml air injection. So, there were a total of 30 videos from this experiment, which were then run on the shape program to get an estimated bubble diameter and number of bubbles. The bubbles were also counted manually for each of the videos and the total count was

then compared with the new program bubble count with bubble diameters (data shown in the Results and Discussion section, Table 12). From the calibration data, it was observed that in most of the sets the total program bubble volume was nearly half of the 4 ml volume injected.

4.2 Results and Discussion

4.2.1 Eight-Orifice Chamber using Energy method

The new eight-orifice chamber was tested on the eight different fermentation media treatments using the bubble energy program (eight chambers). The HPLC data collected after 4 hours for each of the treatments is shown below in Table 5. Also, the carbon dioxide evolved during the fermentation was computed from the total number of bubbles determined by the energy program, which was then converted to the moles of carbon dioxide as shown in Table 5. To study the reaction kinetics of the fermentation a plot between the HPLC computed ethanol values and the glucose loading values at two yeast levels was plotted (Fig 13 and Fig 14). From Fig 13, the linear equation came out to be y = 1.2037*x + 0.0018. Ideally looking into this equation, it should have taken the form of y = 2*x, showing that when glucose concentration is zero, then ethanol concentration is also zero and any time after that, ethanol concentration is twice as that of glucose on the molar basis. But, at 0.1 g yeast loading, we only got 1.2037*x with an intercept value of 0.0018. This intercept value could be ignored as this accounts to be very small.

However, if we look at the linear equation for the yeast loading of 0.4 g (Fig 14), then the equation was y =1.8285*x - 0.0003. This high yeast case was within 20% of the theoretical 2:1 relationship expected between ethanol and glucose.

Furthermore, we were interested to see how robust this new eight-orifice chamber along with the energy program (eight chambers) was and for this a graph between the energy program value for carbon dioxide moles versus the HPLC measured ethanol value was plotted and is shown in Fig 15. We were expecting to get y = x because of the one to one molar ratio between the carbon dioxide and ethanol produced from fermentation. Instead, we observed highly scattered data with R^2 less than 0.1. The eight-orifice chamber along with the energy program (eight chambers) did not accurately measure the bubble count. The results for each orifice varied considerably for the same glucose loading, which showed that the energy program (eight chambers) for all the eight orifices was limited by the orifice position and web camera to sense the bubbles. Moreover, viewing the videos suggested the bubble sizes were varying due to the pressure fluctuations during the experiment. The irregular bubble size was showing up as opposed to our assumption from the previous single orifice chamber experiments that showed nearly consistent bubble size. This irregularity in size could be because the previous experiments for determining the size used a controlled airflow rate, while the fermentation had an irregular airflow rate, which caused pressure fluctuations inside the headspace, thus caused bubbles with varied diameters. For the computation of

carbon dioxide, we had assumed the bubble volume to the theoretical bubble volume; in reality, they were of varying sizes.

Table 5. Eight fermentation treatment sets with HPLC ethanol and Program carbon dioxide estimation

Treatment set	Orifices	Moles of Ethanol [a]	Mol of Glucose loaded [b]	Bubble # [c]	Volume micro litre [d]	Carbon Dioxide moles [e]
Yeast 0.1 gm						
G	1	0.008	0.005	1659	15959.58	0.0007
G	2	0.009	0.005	3325	31986.50	0.0014
J	3	0.013	0.008	3159	30389.58	0.0014
J	4	0.010	0.008	2270	21837.40	0.0010
G	5	0.009	0.005	3698	35574.76	0.0016
G	6	0.008	0.005	2868	27590.16	0.0012
J	7	0.009	0.008	43	413.66	0.0000
J	8	0.010	0.008	3999	38470.38	0.0017
Yeast 0.1 gm Treatment set						
A	1	0.003	0.002	7045	67772.9	0.0030
A	2	0.003	0.002	5922	56969.6	0.0025
D	3	0.006	0.003	1717	16517.5	0.0007
D	4	0.008	0.003	2554	24569.5	0.0011
A	5	0.003	0.002	2708	26051.0	0.0012
A	6	0.002	0.002	941	9052.4	0.0004
D	7	0.006	0.003	64	615.7	0.0000
D	8	0.005	0.003	1229	11823.0	0.0005

Yeast 0.4 gm Treament set						
I	1	0.009	0.005	1711	16459.82	0.0007
I	2	0.010	0.005	6904	66416.48	0.0030
L	3	0.014	0.008	3776	36325.12	0.0016
L	4	0.013	0.008	3317	31909.54	0.0014
I	5	0.007	0.005	4600	44252.00	0.0020
I	6	0.007	0.005	12840	123520.800	0.0055
L	7	0.015	0.008	600	5772.00	0.0003
L	8	0.015	0.008	3681	35411.22	0.0016
Yeast 0.4 gm Treatment set						
C	1	0.022	0.002	3739	35969.18	0.0016
C	2	0.043	0.002	3603	34660.86	0.0015
F	3	0.065	0.003	7166	68936.92	0.0031
F	4	0.087	0.003	2654	25531.48	0.0011
C	5	0.109	0.002	1821	17518.02	0.0008
C	6	0.130	0.002	4832	46483.84	0.0021
F	7	0.152	0.003	322	3097.64	0.0001
F	8	0.174	0.003	3038	29225.56	0.0013

Note: Moles of Ethanol [a] is HPLC computed value, Moles of Glucose [b] is glucose loading value, Bubble # [c] is bubble count from energy program, Volume microliter [d] is total bubble volume obtained from the multiplication of the bubble count with the theoretical bubble volume and Carbon moles [e] is carbon value predicted from energy program by converting the volume in the molar basis

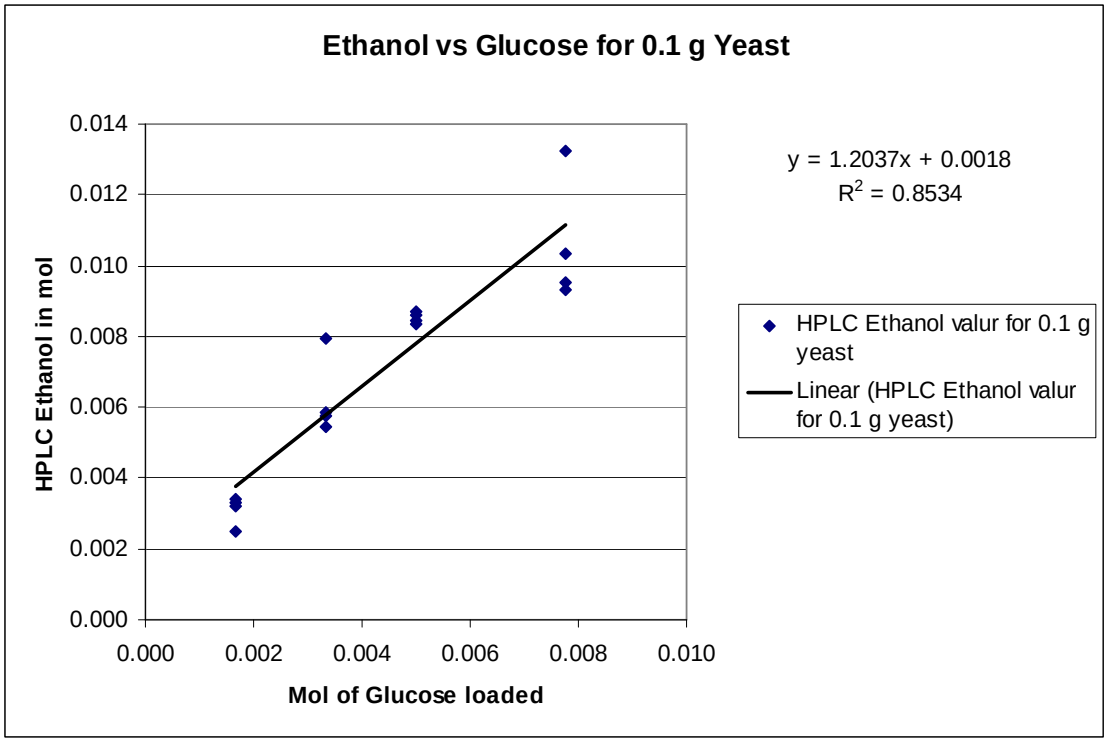

Fig 13. Plot between HPLC computed ethanol in mol and glucose loading in mol at yeast concentration of 0.1 g

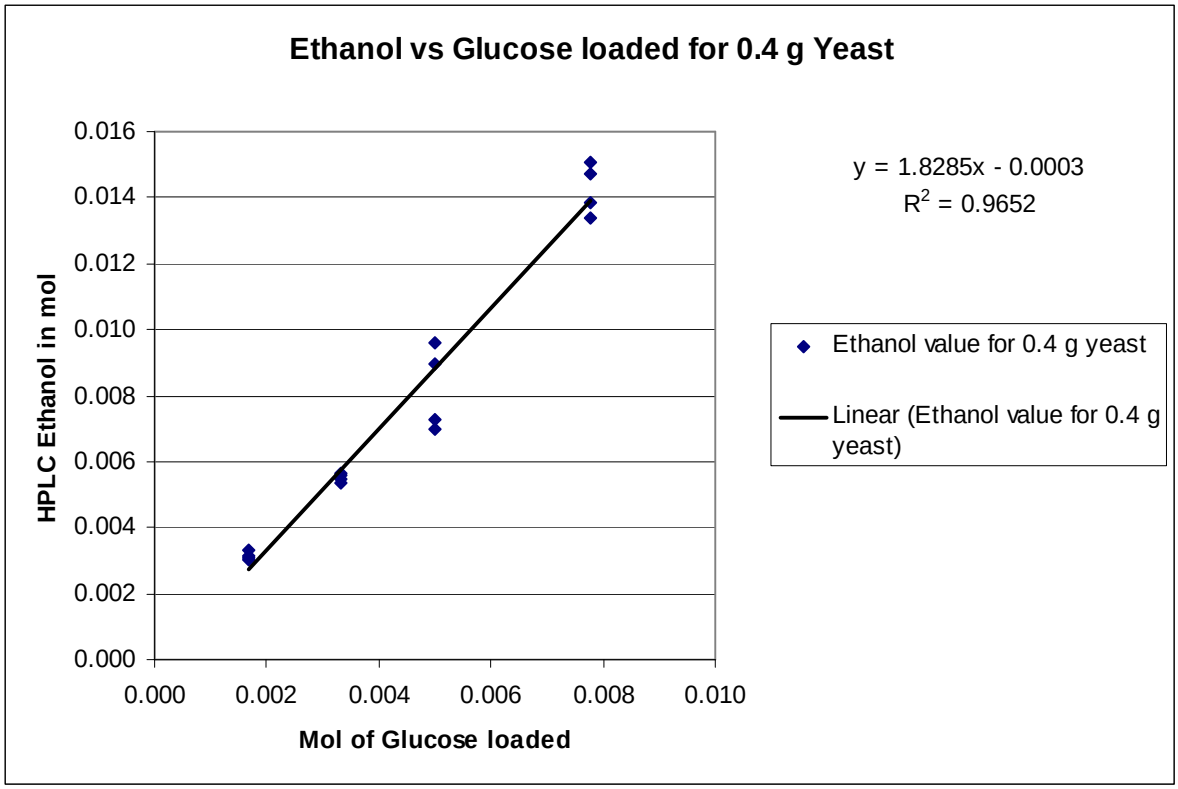

Fig 14. Plot between HPLC computed ethanol in mol and glucose loading in mol at yeast concentration of 0.4 g

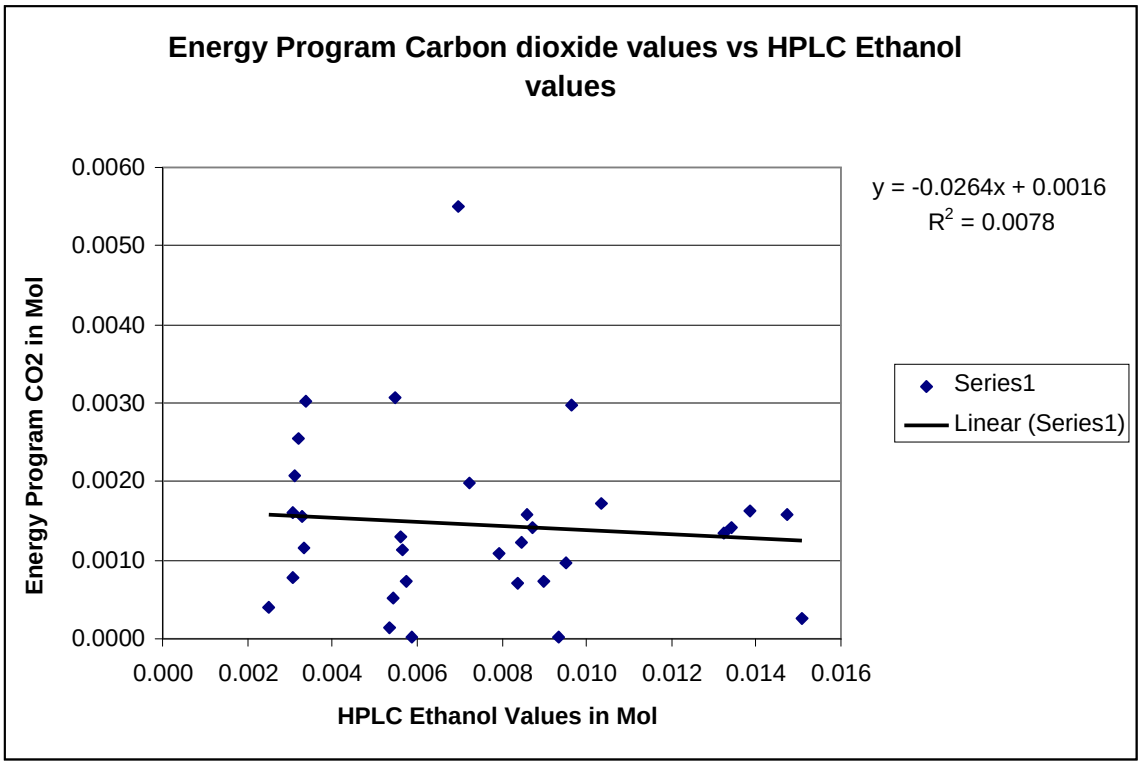

Fig 15. Plot between the Energy program computed carbon dioxide values in mol and HPLC estimated ethanol values in mol.

To have a clear idea of what led to reduced carbon dioxide volume detection, the eight-orifice chamber was tested at the controlled flow rates, which was produced using the syringe pump. The system was tested at four pump positions for 2 ml injected volume in each case. The calibration data for the eight-orifice chamber at four flow rates are presented in Tables 6, 7, 8 and 9. The average bubble count for the manual case at different flow rate was highly scattered. Pump positions 1, 2, 3 and 4 have average manual bubble count of 83, 65, 65 and 63 with 26%, 24%, 27% and 25% of coefficient of variation respectively. For 2 ml of volume injection at four flow rates, nearly 64 bubbles should come out in each case but this does not appear in these data. The program bubble count data for each of the four flow rates had average bubble counts of 69, 60, 60 and 58 with 21%, 25%, 23% and 27% as coefficient of variation. A comparison of the manual and program bubble count data shows that this system counts bubbles close to the manual count as evidenced by the lower coefficient of variations. But, if we compute the average bubble volume using the theoretical volume and average program count, then in this case we got nearly 30% of the injected volume as the bubble volume.

However, if we look at individual orifice bubble count for all the four flow rates, it shows a lot of variation in the bubble count. The possible reason for variation was that the bubbles came out in pair / group and sometimes, the rate of bubble appearance was very fast for the web camera. The web camera operated at 15 frames/sec, and so, if bubbles emerge in a pair or a group, it detected the change in the energy of the frame and counted that as one bubble emergence. The

average of absolute difference of the manual and program bubble count in each of the four positions had 16%, 8%, 9% and 8% percentage of error for flow position of 1, 2, 3 and 4 respectively. From these data, it appears that at low flow rate relating to the position 2, 3 and 4; manual bubble count was in close relation with the program count. An average bubble count of 64 was assumed for 2 ml injection volume and 10% error was assumed. Error more than 10% in the difference of the bubble count was not acceptable and so, was changed to zero value for each of the eight orifices at four flow rates. Then the percentages of error for all eight orifices at individual flow rate were computed and are presented in the Tables 6, 7, 8 and 9. Table 6 shows that at position 1 only three orifices worked fine; position 2 and 3 had six orifices in good working condition (Table 7 and 8), and position 4 had seven orifices providing less bubble count error (Table 9). The reason why position 4 had good number of orifices functioning properly may be due to the small flow rate of 0.10 ml/min and as flow rate was increased from pump position of 3 till 1, the performance of the orifice in the bubble emergence was reduced. At high flow rate, it was observed that bubbles usually emerged in pair/ group and also, at very high rate there was less time difference between the two bubble emergences. So, it was challenging for the web camera to capture very fast rate of change of frames as it was limited for its frame rate.

Further analysis of these data was done by concentrating over each orifice at different flow rates separately for manual and program count. Tables 10 and 11 show the previous data in a modified form. Average variability and coefficient of

variation was computed for each of the eight orifices assuming the 64 bubbles eruption for 2 ml flow volume at four flow rates. Table 10 for manual count, shows that orifice 5 had lot of variability in the performance at different flow rates accounting 136% of average variability of bubble count (average of bubble count at four flow rates divided by 64 bubbles), followed by orifice 8 and 6. However, if we consider the co-efficient of variation for this data set then this was not the case. Orifice 7 had 47% of co-efficient of variation followed by orifice 6 and 4.

Table 6. Manual count and program count at 1.03 ml/min

Position 1 (1.03 ml/min)				
orifice	**Manual count**	**Program count**	**Diff [d]**	**Diff <= 7 [e]**
1	60	59	1	1
2	53	50	3	1
3	70	50	20	0
4	84	83	1	1
5	100	84	16	0
6	109	85	24	0
7	109	75	34	0
8	78	68	10	0
Avg [a]	83	69	14	**38%**
CV [b]	26%	21%		
% error [c]			16%	

Note: a is Average value for the manual and program bubble count, b is co-efficient of variation, c is percentage of error, d is difference between the manual and program count and e is difference value which was less than or equal to 10% of 64 bubble counts.

Table 7. Manual count and program count at 0.412 ml/min

Position 2 (0.412 ml/min)				
orifice	**Manual count**	**Program count**	**Diff**	**Diff <= 7**
1	59	61	2	1
2	50	50	0	1
3	50	46	4	1
4	72	72	0	1
5	69	71	2	1
6	65	46	19	0
7	55	50	5	1
8	96	87	9	0
Avg	65	60	5	**75%**
CV	24%	25%		
% error			8%	

Table 8. Manual count and program count at 0.206 ml/min

Position 3 (0.206 ml/min)

Orifice	Manual count	Program count	Diff	Diff <= 7
1	64	64	0	1
2	58	51	7	1
3	55	56	1	1
4	58	59	1	1
5	97	85	12	0
6	69	68	1	1
7	39	37	2	1
8	81	57	24	0
Avg	65	60	6	**75%**
CV	27%	23%		
% error			9%	

Table 9. Manual count and program count at 0.103 ml/min

Position 4 (0.103 ml/min)

Orifice	Manual count	Program count	Diff	Diff <= 7
1	56	55	1	1
2	53	50	3	1
3	53	39	14	0
4	41	41	0	1
5	82	75	7	1
6	58	51	7	1
7	72	73	1	1
8	85	80	5	1
Avg	63	58	5	**88%**
CV	25%	27%		
% error			8%	

Table 10. Manual counts for each orifice at four flow rates

	Manual Counts					
Orifice no	P1	P2	P3	P4	Avg Val	Co-efficient of Variation
1	60	59	64	56	93%	5%
2	53	50	58	53	84%	5%
3	70	50	55	53	89%	14%
4	84	72	58	41	100%	29%
5	100	69	97	82	136%	22%
6	109	65	69	58	118%	36%
7	109	55	39	72	107%	47%
8	78	96	81	85	133%	12%

Note: P1, P2, P3 and P4 stands for the pump position 1, 2, 3 and 4 respectively.

Avg Val = Average variability in the program count with respect to the 64 bubbles.

Table 11. Program count for each orifice at four flow rates

	Program Values					
Orifice no	P1	P2	P3	P4	Avg Val	Co-efficient of Variation
1	59	61	64	55	93%	6%
2	50	50	51	50	79%	1%
3	50	46	56	39	75%	11%
4	83	72	59	41	100%	28%
5	84	71	85	75	123%	11%
6	85	46	68	51	98%	28%
7	75	50	37	73	92%	29%
8	68	87	57	80	114%	21%

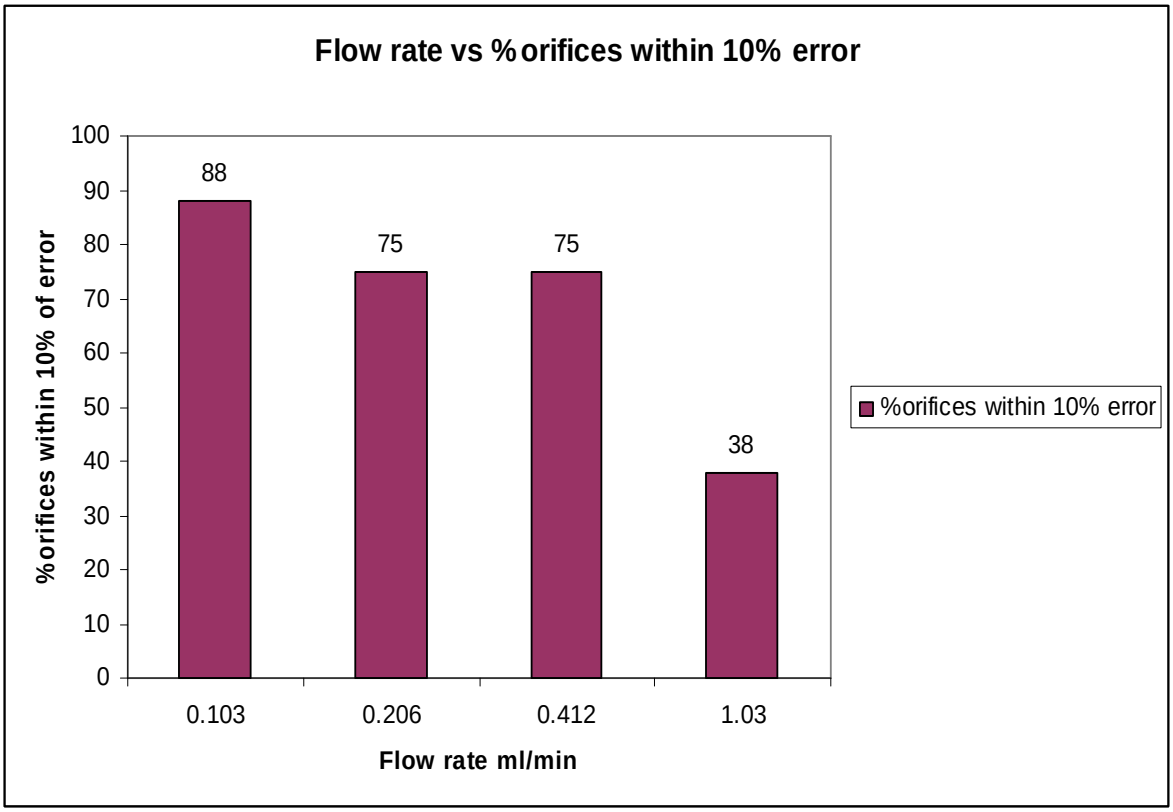

Fig 16. Plot between percentages of orifices working within 10 % of error in manual and program count with respect to the flow rate

4.2.2 Eight-orifice chamber using shape method approach

The bubble detection program was further modified to measure bubble diameter accurately of the emerging bubble when it reaches at the top surface of water, to account for the change in the bubble sizes observed during the previous experiments. While working over the incorporation of the bubble diameter detection with the bubble count technique, orifices 1 and 5 provided false reading during the bubble detection. This was due to their position with respect to the web camera and to poor illumination. So, for the shape program, orifices 1 and 5 were not included. The shape program and the eight orifices chamber were tested at the flow rate of 0.412 ml/min with the injected volume of 4 ml in all the runs. Thirty videos were recorded and were run using the shape program to detect the bubble diameter and the bubble volume for individual bubble. The data for the total bubble volume and the standard deviation for each orifice are shown in the Table 11. The average bubble volume computed using the shape program varied a lot from the injected air volume of 4 mL and from the Table 11, it can be seen that bubble volume from orifice 3 and 6 had exceeded the injected volume, which in reality can not be possible. This means that there were some false positive readings in the bubble count to get the bubble volume through this program. However, the average bubble volumes for the remaining orifices were quite less than the injected volume, which showed that the program missed some of the bubbles or did not detect the bubble edges accurately enough to count for a bubble. Standard deviation for the mean bubble volume was low for orifice 4, followed by orifice 2, but the volume estimation

for orifice 4 was nearly 32% of the injected volume as compared to the orifice 2, which had 64% as the bubble volume.

Table 12. Average volume of bubbles from six orifices using the shape program

Orifice position	Average Bubble Volume (ml)	Standard Deviation
2	2.58	0.25
3	4.68	5.06
4	1.30	0.21
6	8.00	14.07
7	1.46	0.83
8	2.05	1.09

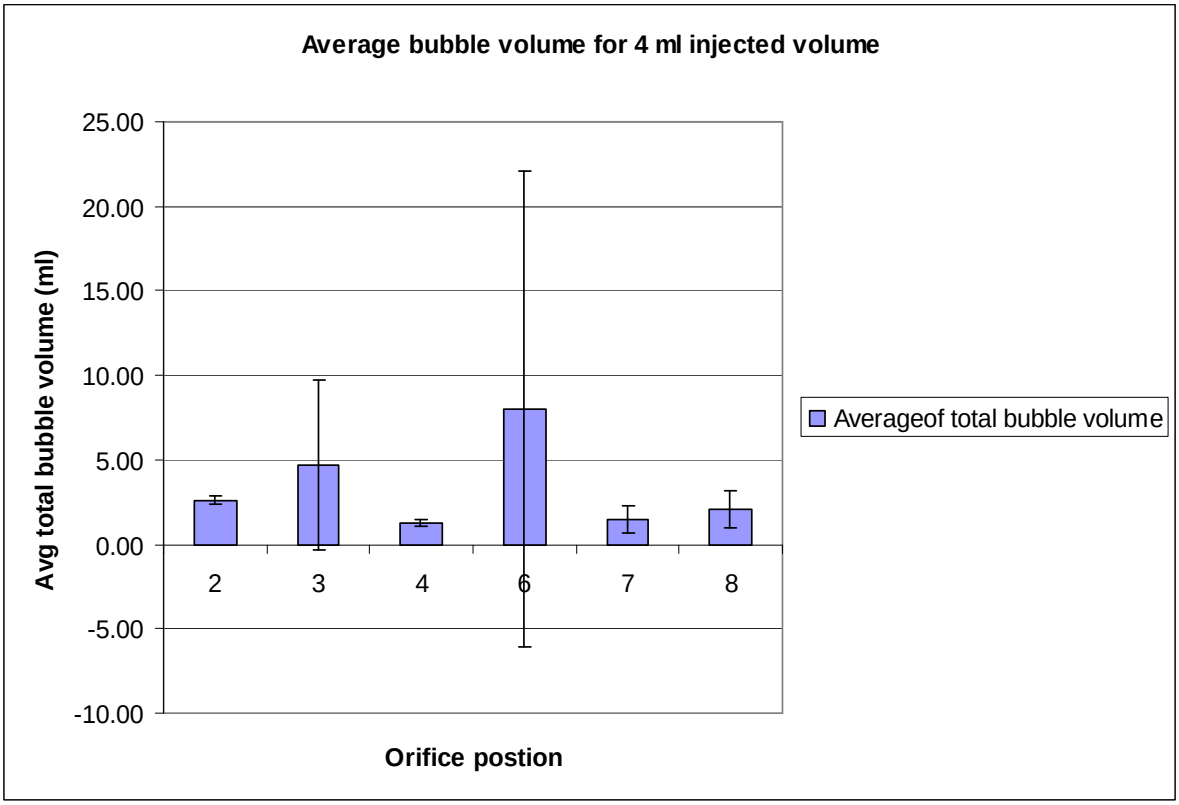

Fig 17. Plot between the average of total bubble volume for each orifice using the shape program.

CHAPTER 5

CONCLUSIONS

The goal of this study was to develop a high throughput ethanol monitoring system incorporating the concept of multi channel bubble based optical system, and testing this system at different sugar and yeast levels and also at varied controlled flow rate comparable to the carbon dioxide evolution rate during the fermentation. This concept was initiated with development and testing of a single orifice chamber at six controlled airflow rates. The bubble volume computed using the energy program for single orifice chamber were in the range of 17% -23% of the injected volume. The single orifice chamber was expanded to the eight-orifice chamber and was tested using the energy program and the shape program. Eight different fermentation sets were used to evaluate the performance of eight-orifice chamber using the energy program. A linear equation fitted over the plot of energy program computed carbon dioxide values and HPLC estimated ethanol values had a negative slope of 0.026, in contrast to the expected outcome of having unit slope. Furthermore, the eight-orifice chamber system was tested with the new shape program and several iterations were done using the shape program, which resulted in the average bubble volume output in the range of 30- 64 % of the injected volume or the actual volume exited through the orifice chamber.

In this work, we were not able to run the web camera at its maximum 30 fps because of software limitations. Future work involves refining of the shape detection

program to accurately measure the bubble diameter and the bubble count. Additionally, it is recommended that a high-speed video camera coupled to a faster video card to be used to support the functioning of the optical sensor at high frame rate. A better illumination system would also improve the system.

REFERENCES

Brown, R. C. 2003. Biorenewable Resources. Engineering New Products from Agriculture. *First Edition*. 54,169.

Byakova, A., T. Nakamura., S. Gnyloskurenko and O. Raychenko. 2005. Influence of wettability on bubble formation in liquid. *Journal of Materials Science*. 40: 2437-2441.

Chen, R. L. C. and K. Matsumoto. 1995. Sequential enzymatic monitoring of glucose, ethanol and glutamate in bioreactor fermentation broth containing a high salt concentration by a multi-channel flow injection analysis method. *Analytica Chimica Acta*. 308:145-151.

Chen, Y.; Sharma, R. R. S.; Keshwani, D. and C. Chen. 2007. Potential of Agricultural Residues and Hay for Bioethanol Production. *Applied Biochemistry and Biotechnology*. 142: 276-290.

Demirbas, A. 2005. Bioethnaol from cellulosic materials: a renewable motor fuel from biomass. *Energy Sources*. 27(4):327-337.

Demirbas, A. 2008. Biofuels sources, biofuels policy, biofuels economy and global biofuels projections. *Energy Conversion and Management*. 49: 2106-2116.

Eliana, M. A., Salgado, A. M., Cos, O., Pereira, N., Valdman, B. and F. Valero. 2007. Enzymatic Microreactors for the Determination of Ethanol by an Automatic Sequential Injection Analysis System. *Applied Biochemistry and Biotechnology*. 136-140:17-25.

Ge, X. M., Zhao, X. Q and F.W. Bai. 2005. Online Monitoring and Characterization of Flocculating Yeast Cell Flocs During continuous ethanol fermentation. *Biotechnology and Bioengineering.* 90(5):523-531.

Gunta, M., Diewok, J., Baena, J. R., Rosenberg, E. and B. Lendl. 2004. Online Fermentation Monitoring by Mid-infrared Spectroscopy. *Applied Spectroscopy*. 58(7):804-810.

Hayes, W. B., B. W. Hardy and C. D.Holland. 1959. Formation of gas bubbles at submerged orifices. *A.I.Ch.E. Journal*. 5(3):319-324.

Kadam, K. L. 2002. Environmental benefits on a life cycle basis of using bagasse-derived ethanol as a gasoline oxygenate in India. *Energy Policy*. 30(5):371-384.

Kostov, Y., P. Harms, L. R. Eichhorn and G. Rao. 2001. Low cost Microbioreactor for High Throughput Bioprocessing. *Biotechnology and Bioengineering*. 72(3):346-352.

Lapa, R. A. S., Lima, J. L. F. C. and I. V. O. S. Pinto. 2003. Development of a sequential injection analysis system for the simultaneous biosensing of glucose and ethanol in bioreactor fermentation. *Food Chemistry*. 81:141-146.

Liu, Y. C.; Wang, F. S. and W. C. Lee. 2001. Online monitoring and controlling system for fermentation processes. *Biochemical Engineering Journal*. 7: 17-25.

Lliadis, P., V. Douptsoglou and M. Stamatoudis. 2000. Effect of orifice submergence on bubble formation. *Chemical Engineering Technology*. 23(4): 341-345.

Malherbe, S. and T. E. Cloete. 2002. Lignocellulosic biodegradation: Fundamentals and applications. *Environmental Science and Bio/Technology*. 1:105-114.

McCarthy, E. J. and M. Tiemann. 1998. MTBE in Gasoline: Clean Air and Drinking Water Issues. *CRS Report for Congress*. CRS1-CRS7.

Perlack, R. D., Wright, L. L., Turhollow, A. F., Graham, R. L., Stokes, B. J. and D. C. Erbach. 2005. Biomass as feedstock for a Bioenergy and Bioproducts Industry: *The Technical Feasibility of a Billion-Ton Annual Supply*. Oak RidgeNationalLaboratory.

http://feedstockreview.ornl.gov/pdf/billion_ton_vision.pdf

Perry, H. R. and C. H. Chilton. 1973. Chemical Engineer's Hanbook. Fifth edition. 18/67 – 18/69.

Raman, D. R and R. P. Anex. 2006. Personal Communication. Dec 2006.

RFS.2007.RenewableFuelStandards,sec.202.
http://www.ethanolrfa.org/resource/standard/

Snabre, P. and F. Magnifotcham. 1998. Formation and rise of a bubble stream in a viscous liquid. *The European Physical Journal B*. 4:369-377.

Sun, Y and J. Cheng. 2002. Hydrolysis of lignocellulosic materials for ethanol production: a review. Bioresource Technology. 83:1-11.

Tkac, J., P. Gemeiner., I. Vostiar and E. Sturdik. 2002. Monitoring of ethanol during fermentation using a microbial biosensor with enhanced selectivity. *Bioelectrochemistry*. 56:127-129.

U.S. Department of Energy Office of Science. Genomics:GTL. *Systems Biology for Energy and Environment.*

http://genomicsgtl.energy.gov/biofuels/benefits.shtml

Varga, E., H. B. Klinke, K. Reczey and A. B. Thomsen. 2004. High solid simultaneous saccharification and fermentation of wet oxidized corn stover to ethanol. *Biotechnology and Bioengineering*. 88(5): 567-574.

Varma, R., B. A. Baliga, V. V. Jogdand and N. G. Karanth. 1999. Online monitoring of ethanol: in relation to the rate of carbon dioxide evolved. *Biotehnology Techniques*. 13:363-364.

Wang, M. 2005. Ethanol: the complete energy lifecycle picture. U.S. Department of energy. http://www.transportation.anl.gov/pdfs/TA/345.pdf

Wang, M; M. Wu and H. Huo. 2007. Life-cycle energy and greenhouse gas emissions impacts of different corn ethanol plant types. *Environmental Research Letters*. 2: 1-13.

Warriner, K., A. Morrissey, J. Alderman, G. King, P. Treloar and P. M. Vadgama. 2002. Modified microelectrode interfaces for inline electrochemical monitoring of ethanol in fermentation processes. *Sensors and Actuators B*. 84:200-207.

Weimer, P. J., Dien, B. S., Springer, T. L. and K. P. Vogel. 2005. In vitro gas production as a surrogate measure of the fermentability of cellulosic biomass to ethanol. *Applied Microbiol Biotechnology*. 67:52-58.